UC Irvine
Faculty Publications

Title
Terrestrial ecosystem production: A process model based on global satellite and surface data

Permalink

Journal

ISSN

Authors
Potter, Christopher S
Randerson, James T
Field, Christopher B
et al.

Publication Date

DOI

Copyright Information

Peer reviewed

TERRESTRIAL ECOSYSTEM PRODUCTION: A PROCESS MODEL BASED ON GLOBAL SATELLITE AND SURFACE DATA

Christopher S. Potter,[1] James T. Randerson,[2] Christopher B. Field,[2] Pamela A. Matson,[3] Peter M. Vitousek,[4] Harold A. Mooney,[4] and Steven A. Klooster[1]

Abstract. This paper presents a modeling approach aimed at seasonal resolution of global climatic and edaphic controls on patterns of terrestrial ecosystem production and soil microbial respiration. We use satellite imagery (Advanced Very High Resolution Radiometer and International Satellite Cloud Climatology Project solar radiation), along with historical climate (monthly temperature and precipitation) and soil attributes (texture, C and N contents) from global (1°) data sets as model inputs. The Carnegie-Ames-Stanford approach (CASA) Biosphere model runs on a monthly time interval to simulate seasonal patterns in net plant carbon fixation, biomass and nutrient allocation, litterfall, soil nitrogen mineralization, and microbial CO_2 production. The model estimate of global terrestrial net primary production is 48 Pg C yr^{-1} with a maximum light use efficiency of 0.39 g C MJ^{-1} PAR. Over 70% of terrestrial net production takes place between 30° N and 30° S latitude. Steady state pools of standing litter represent global storage of around 174 Pg C (94 and 80 Pg C in nonwoody and woody pools, respectively), whereas the pool of soil C in the top 0.3 m that is turning over on decadal time scales comprises 300 Pg C. Seasonal variations in atmospheric CO_2 concentrations from three stations in the Geophysical Monitoring for Climate Change Flask Sampling Network correlate significantly with estimated net ecosystem production values averaged over 50°-80° N, 10°-30° N, and 0°-10° N.

[1]Johnson Controls, NASA Ames Research Center, Moffett Field, California.
[2]Carnegie Institution of Washington, Department of Plant Biology, Stanford, California.
[3]NASA Ames Research Center, Moffett Field, California.
[4]Department of Biological Sciences, Stanford University, Stanford, California.

INTRODUCTION

The amount of carbon fixed annually via terrestrial net primary productivity (NPP) or released by soil microbial respiration (R_s) is about an order of magnitude greater than the annual increase in atmospheric carbon dioxide (CO_2) levels due to fossil fuel combustion [Ajtay, 1979; Houghton et al., 1992]. Seasonal changes in the balance between photosynthetic carbon fixation by land plants and microbial respiration are of a size sufficient to drive the intra-annual oscillation of atmospheric CO_2 concentration [Bacastow et al., 1985; Houghton, 1987]. Either carbon fixation or respiration could be affected substantially by components of global change (e.g., warming or elevated CO_2 concentrations), which raises the possibility of long-term modifications in the carbon balance of terrestrial ecosystems [Rastetter et al., 1991; Mooney et al., 1991] and feedbacks to global biogeochemistry and radiative forcing.

Most ecosystem-level understanding about the magnitude of CO_2 exchange with the terrestrial biosphere is based on correlations between measured fine-scale fluxes and climate characteristics [Friedlingstein et al. 1992; Raich and Schlesinger, 1992]. Satellite remote sensing can be used to extend this information; for example, the normalized difference vegetation index (NDVI) from the advanced very high resolution radiometer (AVHRR) has been used to estimate NPP and seasonal exchange of CO_2 between the atmosphere and the terrestrial biosphere [Tucker et al., 1986; Fung et al., 1987; Heimann and Keeling, 1989].

Many of the fundamental questions about the global carbon cycle can be addressed using simulation models that operate on a scale that links remote sensing, spatial data bases of climate and soils, and mechanistic understanding of atmosphere-plant-soil biogeochemistry. In this paper, we describe the development and application of the Carnegie-Ames-Stanford approach (CASA) Biosphere model for study of the terrestrial carbon cycle. Our overall objective was to characterize fixation and release of CO_2 using spatially (1° latitude-longitude) and temporally (monthly) resolved predictions of steady state net ecosystem production (NEP), the difference between NPP and R_s.

MODELING APPROACH

The model runs on a monthly time interval to simulate seasonal patterns in net plant carbon fixation, biomass and nutrient allocation, litterfall, soil nitrogen mineralization, and CO_2 production. A

schematic representation of data input and ecosystem model integration is shown in Figure 1. Our fundamental approach was to define optimal metabolic rates for major ecosystem biogeochemical processes and to adjust these spatially uniform variables using unitless scalars related to the effects of air temperature, predicted soil moisture, litter substrate quality (N and lignin contents), soil texture, and land use. The coupled plant production and soil microbial respiration components of the model are regulated by a common soil moisture submodel. The model's NPP component is based on the concept of light-use efficiency explored by Monteith [1972, 1977]. The soil component simulates carbon and nitrogen cycling using a set of compartmental difference equations with a structure comparable to a somewhat simplified version of the CENTURY model [Parton et al., 1987, 1988]. Model input and state variables are stored as raster map arrays in a geographic information system (GIS). Major variables are defined in the appendix.

GLOBAL DATA SETS

All global data sets used as inputs to the model (Table 1) were resampled (if necessary) to a 1°x1° spatial resolution. Specific data sources are described in the following paragraphs.

Vegetation Index

We used monthly NDVI-FASIR (defined below) data sets for 1987 processed by Los et al. [1993] and Sellers et al. [1993]. This FASIR product includes a
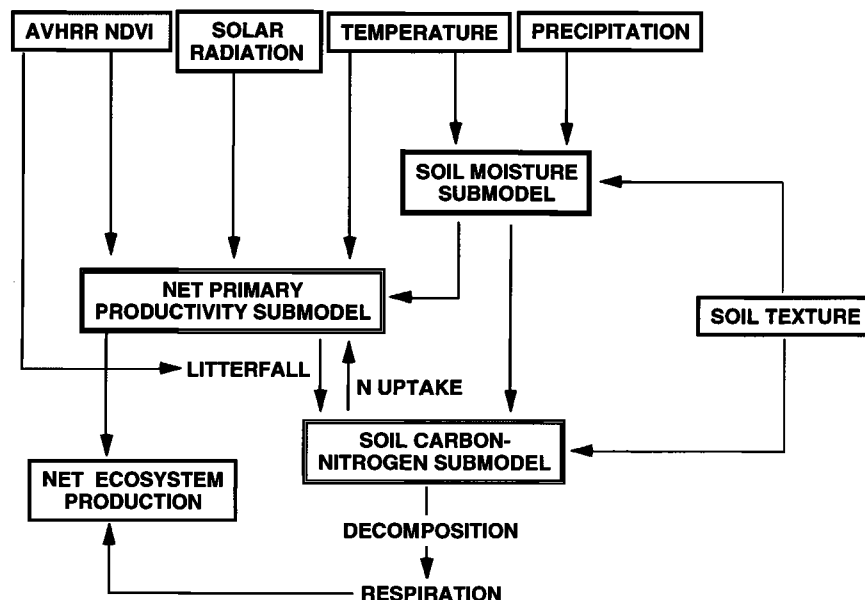

Fig. 1. Model integration framework. Global climate data sets are combined with soil texture settings to compute the monthly water balance, which controls NPP and soil microbial activity.

TABLE 1. Global Geographic Data Sets Used the Model

Name	Attributes	Source[a]	Resolution[b]	Reference
TEMP/PPT	Monthly temperature and precipitation	IIASA	0.5°x0.5°	Leemans and Cramer [1990]
SOLAR	Monthly 1987 solar radiation	GISS	5°x5°	Bishop and Rossow [1991]
NDVI	Monthly 1987 FAS/FASIR	GSFC	1°x1°	Los et al. [1993]
SIBVEG	Vegetation types	GSFC	1°x1°	Dorman and Sellers [1989]
GZTEX	FAO soil texture groups	GISS	1°x1°	Zobler [1986]
SOILC	Soil carbon densities	ARC/IIASA	0.5°x0.5°	Post et al. [1985] Leemans [1990]
SOILN	Soil nitrogen densities	ARC/IIASA	0.5°x0.5°	Post et al. [1985] Leemans [1990]

[a]Institutional sources of geographic data sets: ARC, NASA Ames Research Center, Moffett Field, California; GISS, NASA Goddard Institute for Space Studies, New York, New York; GSFC, NASA Goddard Space Flight Center, Greenbelt, Maryland; and IIASA, International Institute for Applied Systems Analysis, Laxenburg, Austria.
[b]Original resolution of gridded data.

Fourier adjustment (FA) to eliminate many effects of cloud contamination, a solar zenith angle correction (S), an interpolation (I) to prevent boreal forests from dropping to zero during winter months, and a reconstruction (R), in which all monthly values for evergreen tropical forests are held at the yearly maximum for those pixels. The reconstruction step eliminates further cloud interference that is characteristic of AVHRR-global area coverage (GAC) data for areas with frequent convective cloudiness. To identify the month of maximum NDVI and for estimation of the timing of litterfall, we used the FAS product which does not include I and R treatments.

Radiation

Solar radiation (W m^{-2} mo^{-1}) data sets used in the model were computed surface irradiance from the International Satellite Cloud Climatology Project (ISCCP) [Bishop and Rossow, 1991]. They combine estimates of atmospheric optical depth from the ISCCP with calculations from a simplified general circulation model (GCM) transfer scheme to estimate monthly surface irradiance. These data have an accuracy of 9 W m^{-2} on a daily basis and less than 4% bias in the 17-day mean relative to ground measurements.

Climate

The historical climate data sets we used were compiled by Leemans and Cramer [1990], who included stations with at least five years of

observations during period 1930-1960. Leemans and Cramer [1990] corrected the temperatures for altitude by combination of an estimated adiabatic lapse rate with global topographic coverage. The coverage quality of the data is considered best for Europe, North America, East Asia and Japan. We interpolated the data from Leemans and Cramer [1990] from their original 0.5°x0.5° resolution to 1°x1° using bi-directional splining.

Vegetation Characterization

We used the characterization of vegetation type from Dorman and Sellers [1989], modified as described in Sellers et al. [1993]. It is a simplified physiognomic classification based on the world vegetation classes of Kuchler [1983] and the land use database of Matthews [1984, 1985]. We use this classification system in the CASA model for two reasons: (1) It aggregates to a manageable number (12) of vegetation classes; and (2) Unlike other vegetation classification systems which are oriented toward ecologically based descriptions of the plant cover, the Dorman and Sellers [1989] classification is based on plant energy balance and life form dynamics, as these are most useful for coupling the land surface with atmospheric chemistry and physics. Areal extent and latitude zone distributions of the 12 vegetation classes are shown in Table 2.

Soil Type and Texture

Our model used the FAO/UNESCO [1971] Soil Map of the World (SMW) for characterization of soil

TABLE 2. Areas and Distributions of Global Vegetation Classes

Class	Description	n	Area, 10^6 km^2	%Land Cover	Latitude Zone Distribution (% Cover) North, deg 90-60	60-30	30-0	South, deg 0-30	30-60
1	Broadleaf evergreen trees	1433	17.4	11.7	0	1	46	53	0
2	Broadleaf deciduous trees	258	2.3	1.5	0	75	14	0	11
3	Broadleaf and needleleaf trees	487	3.9	2.6	6	85	0	1	7
4	Needleleaf evergreen trees	2156	14.9	10.0	37	59	3	0	1
5	Needleleaf deciduous trees	1117	6.2	4.2	74	26	0	0	0
6	Broadleaf trees with groundcover	1582	18.2	12.2	1	14	27	55	3
7	Perennial grasslands	951	10.5	7.0	2	28	36	30	3
8	Broadleaf shrubs with grasslands	194	2.3	1.5	0	14	21	56	9
9	Broadleaf shrubs with bare soil	911	9.5	6.4	0	45	24	15	15
10	Tundra	1252	6.0	4.0	92	8	0	0	0
11	Bare soil and desert	1589	16.0	10.7	12	24	53	10	0
12	Cultivation	2783	26.4	17.7	0	67	15	6	12
13	Ice	7384	15.5	10.4					
Total		22097	149.0	100.0					

texture classes and their associated particle size distributions (Table 3). Data used to construct the SMW has been assembled from actual soil surveys (21% of global coverage); field reconnaissance of topography, geology, vegetation and climatic data (40% of global coverage); and general information from the local literature (39% of global coverage) [Gardiner, 1982]. Substantial disparities in the reliability of soil type classification have been identified over areas of tropical Central and South America and Africa [Gardiner, 1982; Richter and Babbar, 1991].

Soil Carbon and Nitrogen Contents

We created global gridded data sets by mapping Holdridge [1967] life zone soil C and N content (g m^{-3}) averages reported by Post et al. [1985] to their corresponding life zone categories produced by Leemans [1990]. Spatial interpolation of the resulting data sets from 0.5° to 1.0° latitude/longitude was accomplished using bi-directional splining, preceded by nearest-neighbor fill to conserve land-water boundary elements. Soil profiles used in this data set were all from natural vegetation and excluded wetlands. Post et al. [1985] considered coverage of the original data to be best for tropical and cool temperate forests; coverage is poorer over extremely wet areas, dry tundra, dry boreal and warm desert life zones.

Other Variable Definitions

Ranges of certain other model variables were estimated from the literature, as discussed below.

These include leaf:root:wood C and N allocation ratios, litter and soil organic matter decomposition rates, and C assimilation efficiency of microbes. To simplify interpretations in this version of the model, we set spatially uniform values for most of these variables. As part of the modeling process, uniform rate constants related to photosynthesis and microbial respiration fluxes are adjusted for temporally and spatially resolved stress effects.

MODEL STRUCTURE

Net Primary Productivity

New production of plant biomass (NPP) at a grid cell (x) in month t is a product of intercepted photosynthetically active radiation (IPAR) and a light utilization efficiency (ε) that is modified by temperature and soil moisture (equation (1)). Neither IPAR nor ε is dependent on ecosystem type.

$$NPP(x,t) = IPAR(x,t) \; \varepsilon(x,t) \qquad (1)$$

Monteith [1972, 1977] introduced models that estimate crop growth from IPAR. Subsequent empirical studies documented that ε varies over a relatively narrow range for crop ecosystems (1.1 - 1.4 g C MJ^{-1} PAR) but over a wider range for natural ecosystems [Russell et al., 1989]. Monteith's model incorporated the possibility of variation in ε by making it a function of temperature, water, and nutrient stress.

IPAR is given by

TABLE 3. Soil Characteristics Estimated for FAO Texture Classes

Class	%Clay[a]	%Silt[a]	%Sand[a]	FC[b]	WP[c]	A[d]	B[d]	Soil C:N[e]
Coarse	9	8	83	0.51	0.20	0.002	-5.48	16
Coarse/medium	20	20	60	0.46	0.26	0.002	-6.54	14
Medium	30	33	37	0.60	0.34	0.013	-6.57	13
Medium/fine	48	25	27	0.65	0.43	0.006	-9.47	11
Fine	67	17	17	0.62	0.47	0.004	-13.78	10

Organic soils were assigned to the coarse/medium texture class [Bouwman et al., 1993].

[a]From Zobler [1986]

[b]Field capacity (m) for forested grid cells; FC(x) for other vegetation types are 50% of these values. Computed based on equation (2) in the work by Saxton et al. [1986] for soil water tension greater than or equal to 10 kPa. Tension was assumed to be 33 kPa for medium to fine textures and 10 kPa for coarse textures [Papendick and Campbell, 1980].

[c]Wilting point (m) for forested grid cells; WP(x) for other vegetation types are 50% of these values. Computed based on equation (2) in the work by Saxton et al. [1986] for soil water tension equal to 1500 kPa.

[d]From Saxton et al. [1986]; used in calculation of RDR.

[e]On the basis of weighted average particle-size C:N values reported by Anderson et al. [1981], Hinds and Lowe [1980], and Cameron and Posner [1979].

$$IPAR(x,t) = SOL(x,t) \, FPAR(x,t) \, 0.5 \qquad (2)$$

where SOL is the total solar radiation incident on grid cell x in month t, from the database of Bishop and Rossow [1991], FPAR is the fraction of the incoming PAR intercepted by green vegetation, and the factor of 0.5 accounts for the fact that approximately half of the incoming solar radiation is in the PAR waveband (0.4 -0.7 μm) [McCree, 1981].

FPAR is calculated as a linear function of the AVHRR simple ratio (SR), where

$$SR(x,t) = (1+NDVI(x,t))/(1-NDVI(x,t)) \qquad (3)$$

A linear relationship between FPAR and SR is supported by theoretical results from Kumar and Monteith [1981], Sellers [1985, 1987] Sellers et al. [1992] and Choudhury [1987], as well as from empirical studies [Demetriades-Shah et al., 1992a]. We used the SR-FPAR relationships developed by Sellers et al. [1993] to adjust slope and intercept terms in equation (4) for aggregate ecosystem groups.

$$FPAR(x,t) = \min\{ SR(x,t)/[SR_{max} - SR_{min}] - SR_{min}/[SR_{max} - SR_{min}], \\ 0.95\} \qquad (4)$$

where SR_{min} represents SR for unvegetated land areas and is set to 1.08 for all grid cells. SR_{max} approximates the value at which all downwelling solar radiation is intercepted and corrects for effects of canopy architecture and residual cloud contamination. SR_{max} was computed for four aggregate ecosystem groups according the rationale of Sellers et al. [1993]. Using the 98th percentile of SR for ecosystem groups, vegetation classes 1 and 6 were set at 4.14; classes 2 and 3 at 6.17; 4 and 5 at 5.43; 7 through 12 at 5.13. A cap of 0.95 was imposed on FPAR in order to reflect a finite upper limit to leaf area.

The NPP formulation allows for regulation in either of the terms on the right side of equation (1). Several lines of evidence indicate that most of the regulation should be in IPAR, with less in ε. One line of evidence comes from surveys which indicate that NPP of many ecosystem types is highly correlated with the annual integral of NDVI [Goward et al., 1985]. Another is the constancy of ε from many experimental studies of unstressed plants, plus results from several studies indicating that nutrient stress [Garcia et al., 1988] and water stress [Squire et al., 1986] have much larger effects on IPAR than on ε. Field [1991] considers ecological factors that should tend to constrain investments in light harvesting (which are manifested as IPAR) in relation to whatever resource or resources are limiting to growth so that all of the IPAR can be used for growth. A strong relationship between NPP and

IPAR does not necessarily indicate that light is the primary resource limiting to growth [Demetriades-Shah et al., 1992b].

Heimann and Keeling [1989] used a uniform ε of 1.25 g C MJ^{-1} PAR for a global light use efficiency model to calculate an annual terrestrial NPP of 56.4 Pg (10^{15} g) C. With the solar radiation and NDVI data sets we used, this uniform ε of 1.25 g C MJ^{-1} PAR yields an annual global NPP of 185 Pg C yr^{-1}, much above any recent estimates. Independent work suggests that ε is not a universal constant [Russell et al., 1989]. To allow for effects of temperature and water stress on ε, we calculate it as

$$\varepsilon(x,t) = T_{\varepsilon 1}(x,t) \, T_{\varepsilon 2}(x,t) \, W_\varepsilon(x,t) \, \varepsilon^* \qquad (5)$$

where $T_{\varepsilon 1}$ and $T_{\varepsilon 2}$ account for effects of temperature stress, W_ε accounts for effects of water stress, and ε^* is the maximum possible efficiency. The two temperature stress terms serve to depress ε at very high and very low temperatures ($T_{\varepsilon 1}$) and to depress ε when the temperature is above or below the optimum temperature (T_{opt}), where $T_{opt}(x)$ is defined as the air temperature in the month when the FAS NDVI reaches its maximum for the year (derived as shown in Plates 1a-1c). $T_{opt}(x)$ ranges from near 0° C in the Arctic to the mid thirties in low latitude deserts.

$T_{\varepsilon 1}(x)$, which ranges from 0.8 at 0° C to 1.0 at 20° C to 0.8 at 40° C, is given by

$$T_{\varepsilon 1}(x) = 0.8 + 0.02 \, T_{opt}(x) - \\ 0.0005 \, (T_{opt}(x))^2 \qquad (6)$$

For mean monthly temperatures of -10° C and below, $T_{\varepsilon 1}$ is set equal to zero. The basic motivation for including $T_{\varepsilon 1}$ is to reflect the empirical observation that plants in very cold habitats typically have low maximum growth rates [Chapin, 1980; Grime, 1979] and high root biomass [Sala et al., 1993], potentially imposing large respiratory costs. Plants in very hot environments may have high growth rates [Schulze and Chapin, 1987], but the efficiency of light utilization should be impacted by high rates of respiration [Amthor, 1989; Ryan, 1991].

Our $T_{\varepsilon 2}$ term, which reflects the concept that the efficiency of light utilization should be depressed when plants are growing at temperatures displaced from their optimum, has an asymmetric bell shape that falls off more quickly at high than at low temperatures. It is given by

$$T_{\varepsilon 2}(x,t) = 1.1814/\{ 1 + e^{[0.2 \, (Topt(x) - 10 - T(x,t))]} \}/ \\ [1 + e^{[0.3 \, (-Topt(x) - 10 + T(x,t))]}] \qquad (7)$$

$T_{\varepsilon 2}$ falls to half its value at T_{opt} at temperatures 10° C above or 13° C below T_{opt}. The idea behind
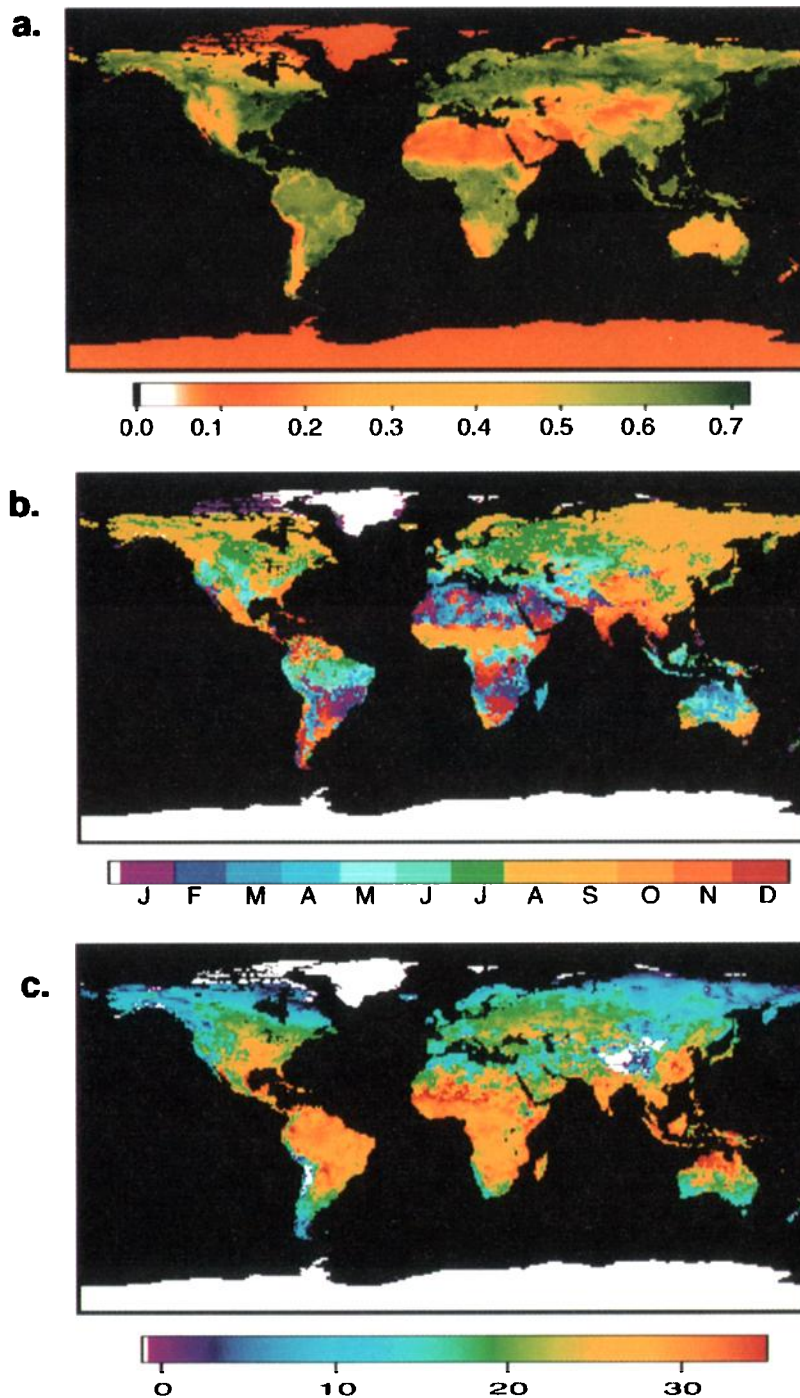
Plate 1. Results from the process of estimation of T_{opt}. (a) FAS-NDVI maximum for each grid cell during the model calibration year of 1987. (b) Month of the year when FAS-NDVI reached its maximum value. (c) Temperature (T_{opt}) during the month of maximum FAS-NDVI; grid cells with T_{opt} less than -1° C are shown in white.

including $T_{\varepsilon2}$ is to capture some of the intrinsic limitations on the flexibility of temperature acclimation. Adjusting T_{opt} to the temperature in the month of maximum NDVI assumes that plant growth is basically adapted to local ambient conditions, but $T_{\varepsilon2}$ reflects the fact that plant temperature responses cannot perfectly track ambient temperatures [Berry and Björkman, 1980].

The water stress factor (W_ε) is calculated as

$$W_\varepsilon(x,t) = 0.5 + 0.5\ EET(x,t)/PET(x,t) \qquad (8)$$

where EET and PET come from the soil moisture submodel. W_ε varies from 0.5 in very arid ecosystems to 1 in very wet ecosystems. For months when T less than or equal to $0°$ C and precipitation accumulates as snow pack on the surface, the W_ε scalar value from the previous monthly time step is carried forward without change. It is similar in form to the water stress control on stomatal conductance in TEM [Raich et al., 1991], but it is less severe. We decreased the severity of the water stress impact on NPP to reflect the observation that most effects of water stress appear in IPAR rather than in ε [Squire et al., 1986].

The maximum efficiency ε^* is set through a single calibration using NPP observed at sites considered by Raich et al. [1991] and McGuire et al. [1992]. The calibration compares the annual observed NPP

(NPP_{obs}) with the annual NPP predicted (NPP_{pred}) for the grid cell that includes each observation site. The ε^* term is calculated through an iterative process that minimizes the following error function.

$$E = \sum_{x=1}^{n} [(NPP_{obs}(x) - NPP_{pred}(x))^2]^{0.5}/NPP_{pred}(x) \qquad (9)$$

where n is 17 observation locations used for calibration and validation by Raich et al. [1991] and McGuire et al. [1992]. An initial estimate for the minimum E in equation (9) was obtained by calculating $NPP_{pred}(x)$ values according to equations (1) and (5) with an ε^* of 0.405 g C MJ^{-1} PAR. This ε^* value is consistent with a total terrestrial NPP of 50 Pg C yr^{-1}. The calibration is similar to calculating ε^* such that the slope of a linear regression of NPP_{pred} versus NPP_{obs} approaches unity. It differs from that, however, in that the minimized term (E) scales with the sum of the deviations divided by the predicted NPP, rather than simply the sum of the squared deviations. Division by NPP_{pred} in equation (9) makes the function sensitive to the proportional, rather than the absolute error in the fit. Because this calibration involves adjustment all the model grid cells by a constant factor, the correlation between model predicted and observed NPP is not affected by the error minimization process.
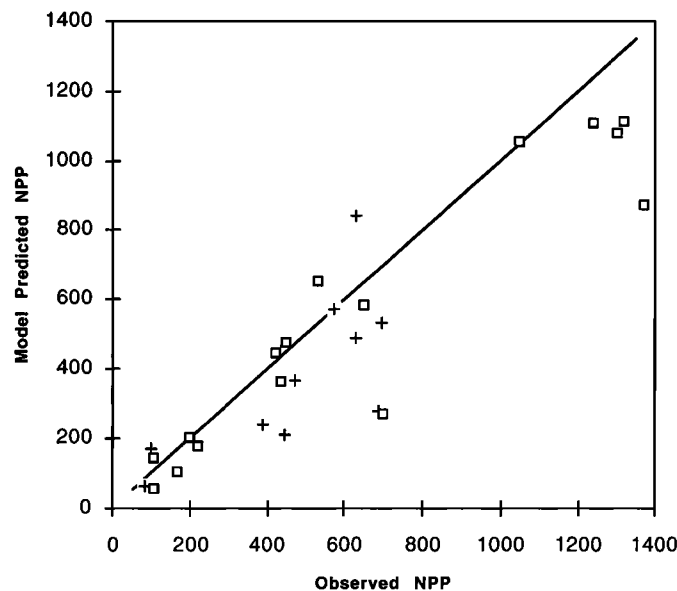

Fig. 2. Model predicted NPP for grid cells containing *in situ* NPP observations. Units are g m^{-2} yr^{-1}. Site estimates marked with a box were used in a single step calibration to obtain ε^*. These sites are the same as those used to calibrate and validate TEM [Raich et al., 1989; McGuire et al., 1992]. All TEM observational sites were used, with the exception of two (Taita, New Zealand and Guanica, Puerto Rico) that were not contained within land grid cells at a 1°x1° resolution. The 1:1 regression line is shown for predicted versus observed values at TEM calibration sites. Validation sites marked with a plus were not used to calibrate ε^*; names and locations of these sites are listed in Table 4.

When E is minimized, the value of ε^* is 0.389 g C MJ^{-1} PAR. Predicted NPP values for the TEM sites cluster reasonably tightly around the 1:1 line (r^2 of 0.89; $p < 0.001$; Figure 2), with the exception of NPP for Chakia, India, a tropical deciduous forest for which McGuire et al. [1992] estimated root production using the carbon balance approach of Nadelhoffer and Raich [1992]. While our approach does a reasonable job of reproducing the measured NPP at the calibration sites, it is somewhat less satisfactory (r^2 of 0.52; $p < 0.01$) in prediction of NPP at several sites that were not used in calibrating the TEM (also shown in Figure 2 and listed in Table 4).

The motivation for this single step calibration is that we lack the understanding to estimate ε^* from first principles. The maximum photon yield of photosynthesis sets an absolute upper bound on ε^* of approximately 2.88 g C MJ^{-1} PAR [Ehleringer and Björkman, 1977], but this value will always be reduced by saturation in the light response of photosynthesis. At the Harvard Forest, Wofsy et al. [1993] measured a gross primary productivity light use efficiency during summer months of around 1.10 g C MJ^{-1} PAR. A 2:1 ratio of gross primary productivity to net primary productivity would argue for a maximum ε^* of around 0.55 g C MJ^{-1} PAR at Harvard Forest, fairly close to the ε^* obtained through the above calibration.

Soil Moisture Submodel

Soil moisture content was calculated at each grid cell using monthly temperature and precipitation in combination with soil texture data and moisture-holding capacity [Saxton et al., 1986]. This submodel is a one-layer "bucket" formulation that builds on previous simulation studies of regional and global surface hydrology [Mintz and Serafini, 1981; Vörösmarty et al., 1989; Bouwman et al., 1993].

Monthly soil moisture storage is calculated for each grid cell (x) as a state variable, SOILM, with the potential to accumulate moisture over several months.

$$\text{SOILM}(x,t) = \text{SOILM}(x,t\text{-}1) - [\text{PET}(x,t) - \text{PPT}(x,t)] \text{ RDR}$$
$$\text{For PPT}(x,t) < \text{PET}(x,t) \qquad (10a)$$

$$\text{SOILM}(x,t) = \text{SOILM}(x,t\text{-}1) + [\text{PPT}(x,t) - \text{PET}(x,t)]$$
$$\text{For PPT}(x,t) \geq \text{PET}(x,t) \qquad (10b)$$

where PPT is average precipitation at month t, PET is potential evapotranspiration at month t, and RDR is a relative drying rate scalar for potential water extraction as a function of soil moisture (SOILM(x,t-1)).

For months when temperature is less than or equal to 0° C, PET and PPT are set equal to zero and there is no net change in SOILM. During these months, precipitation accumulates as snow in a state variable PACK. PACK is added to PPT in the first month that monthly average air temperature (T) > 0° C. This function initiates spring snow melt.

PET is calculated with the method of Thornthwaite [1948]. Lower and upper limits for SOILM were set at wilting point (WPT) and field capacity (FC), respectively (Table 3). These values were derived from soil texture relationships described by Saxton et

TABLE 4. NPP Model Validation Sites

Vegetation	Location	Latitude	Longitude	Reference
Desert shrub	San Simon, Arkansas	31° 50'N	109° 05'W	Chew and Chew [1965]
Grassland	Pantex, Texas	35° 18'N	101° 32'W	Sims and Coupland [1979]
Grassland	Cottonwood, South Dakota	43° 57'N	101° 52'W	Sims and Coupland [1979]
Savanna	Nairobi Park, Kenya	1° 20'S	36° 50'E	Kinyamario and Imbamba [1992]
Forest	Lubumbashi, Zaire	11° 29'S	27° 29'E	DeAngelis et al. [1981]
Oak forest	Oak Ridge, Tennessee	35° 55'N	80° 77'W	DeAngelis et al. [1981]
Forest	Hubbard Brook, New Hampshire	44° 00'N	71° 0'W	DeAngelis et al. [1981]
Forest	Solling, Germany	51° 49'N	9° 35' E	DeAngelis et al. [1981]
Forest-moss	BSMS, Alaska	64° 00'N	128° 00'W	DeAngelis et al. [1981]
Forest	Meathop, United Kingdom	54° 13'N	2° 53'W	DeAngelis et al. [1981]

These sites were chosen according to the following criteria: (1) Above and below ground NPP data were available. (2) Latitude and longitude coordinates of the site fell within land-designated model grid cells. (3) Sites were not near large metropolitan areas. (4) Sites were representative of the major ecosystems present within the grid cell.

al. [1986]. A matric potential of -10 kPa is used for calculating FC for coarse textured soils, whereas a -30 kPa potential is used for medium- to fine-textured soils [Papendick and Campbell, 1980].

The soil rooting depth for forests was set to 2.0 m. Grassland, tundra and cultivation classes (7, 10, and 12) were assigned a rooting depth of 1.0 m [Vörösmarty et al., 1989]. Several soil types were treated as special cases in assigning FC classes. Vertisols and ferrasols were assigned to the medium texture FC class, whereas andosols were assigned to the fine texture FC class [Bouwman et al., 1993]. Lithosols were assigned to a shallow soil class of 27% FC (total soil volume) with rooting depth of 0.1 m [Vörösmarty et al., 1989].

Additions to SOILM that exceed field capacity are assumed to leave the grid cell as runoff. There are no grid-cell interactions in the soil moisture submodel (i.e., runoff from one cell is not transferred to an adjacent cell).

Estimated evapotranspiration (EET) is calculated for each grid cell as

$$EET(x,t) = \min\{PPT(x,t)+[PET(x,t)-PPT(x,t)] \\ RDR\}, \{PPT(x,t)+[SOILM(x,t-1)- \\ WPT(x)]\}$$
$$\text{For } PPT(x,t) < PET(x,t) \qquad (11a)$$

$$EET(x,t) = PET(x,t)$$
$$\text{For } PPT(x,t) \geq PET(x,t) \qquad (11b)$$

Previous studies have shown that the rate of soil drying generally decreases with decreasing soil

moisture content and increasing soil water tension [Thornthwaite and Mather, 1957; Pierce, 1958; Pastor and Post, 1984]. We have fitted a family of logistic drying curves (Figure 3) for derivation of the RDR scalar using a transformation (equation (12)) of the relationship between soil water potential and volumetric moisture content presented by Saxton et al. [1986].

$$RDR = (1+a) / (1 + a \; \Theta^b) \qquad (12)$$

where a and b are texture-dependent empirical coefficient and Θ is the volumetric moisture content (m/m).

These curves resemble texture-dependent drying functions proposed previously [Holmes, 1961; Zahner, 1967]. Their forms imply that EET, a fraction of PET, is reduced dramatically for coarse and fine textured soils as Θ falls below 0.4 and 0.8, respectively. For any month that PPT-PET is greater than zero, RDR is set to unity. When PET exceeds PPT, the potential loss of moisture from SOILM is adjusted by the RDR scalar, which is calculated according to the value of Θ at t-1.

Temperature and Moisture Effects on Microbial Respiration

The effect of temperature on soil C and N fluxes (T_s) was treated uniformly as an exponential (Q_{10}) response (equation (13)) using a Q_{10} value of 2.0 [Fung et al., 1987; Anderson, 1991; Townsend et al., 1992].
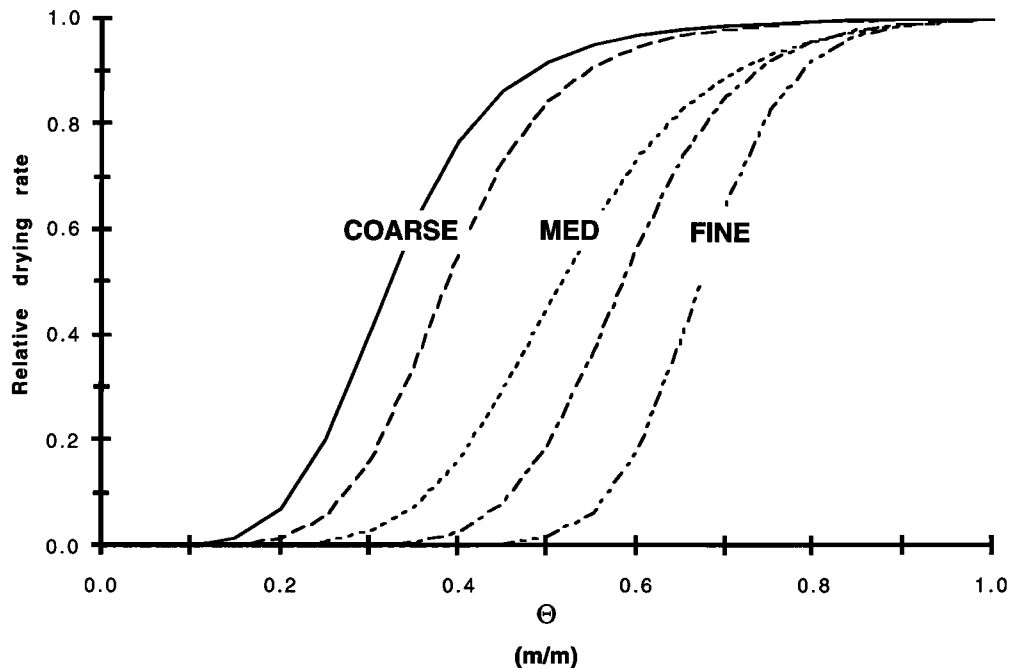

Fig. 3. Soil drying curves derived using a mathematical transformation equation (12) of the relationship between soil water potential and volumetric moisture content presented by Saxton et al. [1986].

$$T_s(x,t) = Q_{10}^{((T(x,t)-30)/10)} \tag{13}$$

where Q_{10} is the multiplicative increase in soil biological activity for a 10° C rise in soil temperature and $T(x,t)$ is monthly average air temperature. Air temperature maxima in the global data inputs truncate the T_s function at 45° C.

A scalar for soil moisture content effects on soil C and N fluxes (W_s) is computed as the ratio of monthly PPT+soil water storage-to-monthly PET (Figure 4). This variable requires estimation of the absolute amount of soil water storage. Therefore, for lithosols, the computation considers soil water storage to 0.1 m in the soil profile; for all other soil types, moisture stored to 0.3 m is considered. The general shape of the moisture function is similar to that used by Parton et al. [1992]. Stress is greatest as rainfall goes to zero, diminishes to its lowest levels at ratio values of 1-2, and increases gradually again under conditions of surplus water supply. As in the calculation of plant moisture stress, when T is less than or equal to 0° C, the scalar value from the previous monthly time step is carried forward without change.
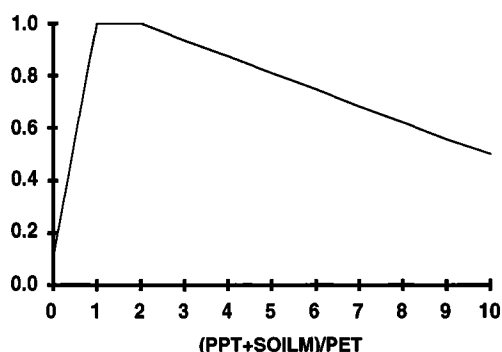
Fig. 4. Scalar function for effect of moisture on soil C/N transformations.

Carbon and Nitrogen Allocation and Litterfall

Allocation of available C among plant tissues in forest vegetation types is currently treated as a fixed partitioning ratio of 1:1:1 among leaf, fine roots and wood [Running and Coughlan, 1988]. For grasslands, carbon is allocated 1:1 between leaf and root pools. In all vegetation types, allocation of N among litter pools is calculated so as to first satisfy fixed pool C-to-N ratios of *structural* (slowly decomposing cellulose plus lignin) leaf and fine root (C:N 150) and woody pools (C:N 260); residual N is partitioned equally between *metabolic* (rapidly decomposing cytoplasmic constituents and nucleic acids) leaf and fine root pools.

Annual NPP is distributed over the months as inputs to the soil C/N submodel in the form of litterfall. Monthly litterfall fractions (LT_{LAI}) are added to standing leaf, fine root and woody litter

pools in proportion to month-to-month changes in leaf area index (ΔLAI). LAI fields were generated according to the calculations described by Sellers et al. [1993]. For homogeneous vegetation types (classes 1, 2, 6, 7, 8, 10, 11, and 12), Sellers et al. [1993] use an exponential relation between FPAR and LAI, whereas for clustered vegetation (classes 4, 5, and 9) they use a linear relation. For grid cells in which there is a combination of clustered and evenly distributed vegetation (class 3), they use a weighted combination of the exponential and linear functions.

These gridded (1°x1°) data sets were used determine LT_{LAI} as the sum of two terms

$$LT_{LAI}(x,t) = NPP_{ann}(x) [LT_{con}(x) + LT_{var}(x,t)] \tag{14a}$$

where $LT_{con}(x) = [LAI_{min}(x)/LAI_{ave}(x)]/12$ (14b)

and $LT_{var}(x,t) = [\Delta LAI_n(x,t)/ \Sigma \Delta LAI_n] [1 - \{LAI_{min}(x)/LAI_{ave}(x)\}]$ (14c)

NPP_{ann} is total annual NPP. The LAI_{min} and LAI_{ave} terms are the minimum and the average of 12 monthly LAI values, respectively. When LT_{con} is greater than zero, a fraction of NPP is distributed evenly throughout the year. The LT_{var} term was computed from annual $\Sigma \Delta LAI_n$, the sum of all monthly time steps for which the difference between month t and month $t-1$ was less than zero. For completely deciduous grid cell locations, the LT_{con} term is zero. For completely constant evergreen grid cells, the LT_{var} term drops to zero for all months. In the model experiments discussed here, it was assumed that no leaves remain in the canopy longer than one year, that the timing of leaf, root, and wood litterfall is synchronous, and that senescent plant material immediately enters litter pools.

Litter C-to-N ratios are continually adjusted over the course of a model run in accordance with computed annual totals of available mineral nitrogen and a prescribed maximum leaf nitrogen concentration (Table 5; based on values reported by Rodin and Bazilevich [1967], Titlyanova and Bazilevich [1979], Coupland and Van Dyne [1979], Cole and Rapp [1981], Gosz [1981], Heal et al. [1981]). Mineralized N (MIN_n) available to vegetation (in excess of the amount needed to meet total N litter, microbial and soil pool demands; see section below) is transferred to monthly plant production (NPP) up to the amount needed to produce litter of the highest N quality (lowest possible C-to-N ratio). If the size of the MIN_n pool is less that the amount needed to support NPP at the highest possible litter quality level, the contents of the MIN_n pool is transferred to NPP, and the C-to-N ratio of NPP floats upward accordingly. Because we assumed that our NPP estimates largely account for effects of N limitation, no minimum N level is set for new production. Total N returned in litterfall is calculated according to the yearly amount of woody

and nonwoody biomass produced divided by mineral N uptake over the previous 12 months. This continually updated ratio is used in combination with fixed (biome specific) lignin levels (Table 5) to partition litterfall into structural and metabolic subpools (see following sections).

Soil Carbon and Nitrogen Fluxes

Major soil carbon-nitrogen pools in the model and transformation processes connecting them at the

TABLE 5. Litter Quality Settings for
Vegetation Classes

Class	Minimum CN	%Lignin
1	25	20
2	25	20
3	25	20
4	25	20
5	25	20
6	15	20
7	15	10
8	15	20
9	25	20
10	15	20
11	15	5
12	15	5

See text for sources.

ecosystem level are shown in Figure 5. Production of CO_2 results from microbially mediated decomposition of plant and soil organic residues, as shown in the following generic equation for C loss from any pool.

$$CO_2(x,t)_i = C(x,t)_i \, k_i \, W_s(x,t) \, T_s(x,t) \, (1-M_\varepsilon) \quad (15)$$

where $C(x,t)_i$ = carbon content of pool i;
  k_i = maximum decay rate constant of pool i;
  $W_s(x,t)$ = scalar for the effect of soil moisture content on decomposition;
  $T_s(x,t)$ = scalar for the effect of temperature on decomposition;
  M_ε = carbon assimilation efficiency of microbes.

Carbon is transferred to microbial pools (or from microbial pools to soil carbon pools) in amounts computed according to equation (15) with M_ε in place of $(1-M_\varepsilon)$. Emissions of CO_2 to the atmosphere from soil microbial respiration are not impeded by snow cover [Stohlgren, 1988; Taylor and Jones, 1990].

Soil nitrogen transformations are tied to carbon fluxes following the basic structure of several previous models [Jenkinson and Rayner, 1977; McGill et al., 1981; Parton et al., 1987]. Leaf and fine root litter inputs are divided initially into metabolic and structural fractions according to the lignin-to-nitrogen ratio of the residue (equation(16)) [Parton et al., 1987].
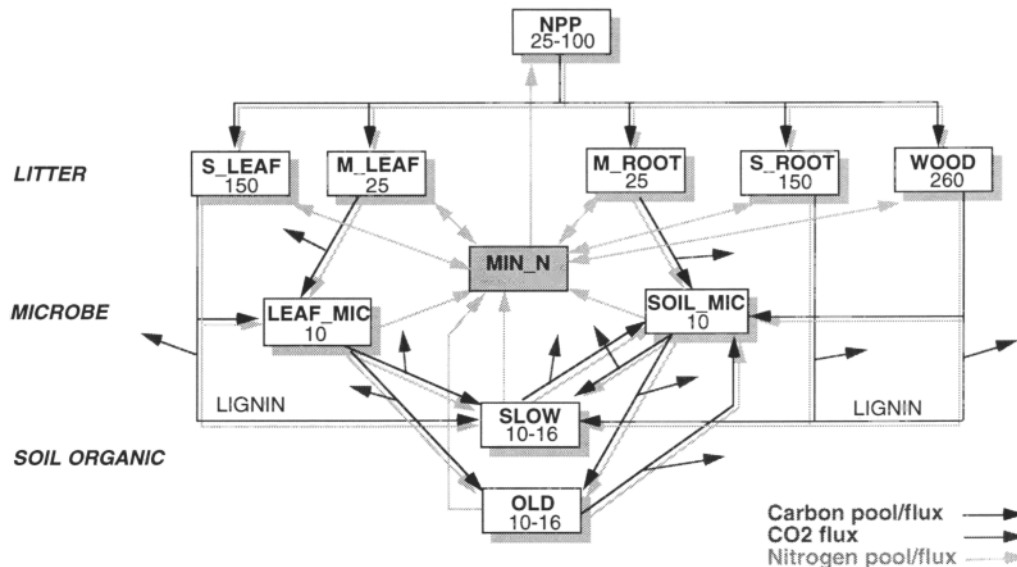

Fig. 5. Ecosystem carbon-nitrogen model. Carbon pools are outlined in black and labeled with C-to-N ratios, C fluxes in solid arrows, CO_2 production in stippled arrows; Nitrogen pools in gray, N fluxes in gray arrows. Levels of litter, microbe (MIC), and soil organic (SLOW and OLD) pools are shown. Structural (S) and metabolic (M) pools are shown for leaf and root litter.

$$MT_f(x,t) = 0.85 - [0.018 \, LN(x,t)] \qquad (16)$$

where MT_f is the fraction of litter that is metabolic and LN is the lignin-to-nitrogen ratio of nonwoody litter. All lignin in residue is assumed to reside in structural fractions.

Leaf (LF), fine root (RT), and woody (WD) plant residues, along with surface and soil microbial (MIC) pools, are represented in the model. The remaining soil carbon and nitrogen resides in SLOW and OLD pools, which represent chemically recalcitrant and physically protected organic matter, respectively. Most soil carbon losses via microbial respiration are based on a M_ε of 45% [McGill et al., 1981]. Lignin, however, bypasses microbial assimilation and cycles directly to the SLOW pool with only 30% C lost to respiration [Stott et al., 1983; Parton et al., 1987].

Maximum decomposition rate constants (k, mo^{-1}) for LF and RT litter, microbial and soil organic matter pools are adjusted to monthly basis (see appendix) from data by Parton et al. [1987]. The maximum turnover rate of woody detritus is uniform globally, with a k value equal to 0.04 mo^{-1} [Harmon et al., 1986; Schowalter, 1992].

Soil texture controls several fluxes. Soil microbial turnover rate decreases in fine textured soils according to equation (17) [Ladd et al., 1981; Sorenson, 1981; Gregorich et al., 1991].

$$ETX(x) = 1 - [0.75 \, SC(x)] \qquad (17)$$

where $SC(x)$ is the silt plus clay fractions.

Second, the fraction of carbon lost as CO_2 from soil microbes during transfer to the SLOW pool ($SLOW_f$) decreases as the soil silt+clay content increases according to the relationship specified in equation (18) [Van Veen et al., 1984; Parton et al., 1987].

$$SLOW_f(x) = 0.85 - [0.68 \, SC(x)] \qquad (18)$$

For initialization of soil pools, we assumed that most of C and N that turns over on decadal-to-century time scales is in the upper 0.3 m of the soil. Hence we set initial soil C and N pool contents (g m^{-2}) using 50% of the totals provided by Post et al. [1985] to 1 m depth for the Holdridge life zone classification of Leemans [1990]. Our model does not consider cycling of the remaining C and N in deeper soil layers. For initialization only, 30% of the total soil C and N contents in the top 0.3 m are allocated to the OLD pool, with the remainder allocated between soil microbial and SLOW pools. Therefore, under this initialization scheme, total ecosystem nitrogen (above and below ground) at each grid cell is constrained by the soil contents specified by Post et al. [1985]. The soil microbial C pool is initialized as a fraction (MIC_f) of soil C contents provided by Post et al. [1985]. We used the

relationship between MIC_f and the ratio of annual PPT-to-PET suggested by Insam et al. [1989], which takes on initial values between 2% and 5%. All other soil pools are initialized at zero.

N Mineralization and Immobilization

Nitrogen transformations are stoichometrically related to C flows. Fluxes from litter and soil to microbial pools and from microbial pools back to soil pools occur in proportion to C assimilation rates so that prescribed C-to-N ratios for the various recipient organic matter pools are maintained [Parton et al., 1987]. Mineralization occurs as carbon-bonded N is released during CO_2 production. Microbial immobilization occurs at rates necessary to meet critical pool C-to-N ratios (levels to which litter accumulates N until release occurs). Berg and Staff [1981] reported a range of critical C-to-N ratios from 25 to 50 for foliar material and up to 170 for more lignified material. Critical C-to-N ratios for leaf and root pools are set at 25 and 150 for metabolic and structural pools, respectively. The critical C-to-N ratio for woody litter are set at 260. The C-to-N ratio for fluxes into the two microbial pools is fixed at 10 [Parton et al., 1987], whereas C-to-N ratios of SLOW(x) and OLD(x) pools are soil texture dependent. Soil C:N values range from 7 to 20 for predominately clay to sand particle-size fractions, respectively [Chichester, 1969]. The C-to-N ratios of soil particle-size fractions have been reported by several workers [Cameron and Posner, 1979; Hinds and Lowe, 1980; Anderson et al., 1981]. Average C:N values from these studies were applied to the size fraction composition of the soil texture classes in the modified FAO soil database [Zobler, 1986] to compute composite C:N for SLOW and OLD pools (Table 3).

Changes in the mineral N pool (MIN_n) reflect the difference between total mineralization inputs that result from N release during microbial CO_2 production, and immobilization outputs needed to meet the critical C-to-N ratios of litter N pools (shown in Figure 5). To avoid the potential for complete depletion of N pools, we fixed the priority for potentially competing N transfers between litter, microbial, soil organic matter, and mineral pools. For example, each of the structural and woody litter pools has three possible paths of N outflow: to $SLOW_n$ via lignin decomposition (S_{n1}); to surface/soil microbes via nonlignin decomposition (S_{n2}); and to the mineral pool (S_{n3}). Provided there is sufficient N available in the structural litter pool, the S_{n1} flow is satisfied first by computing the amount of N needed, relative to the corresponding carbon side flow, to maintain the critical C:N of the SLOW pool. If there is insufficient N available in the structural pool to meet 100% of this demand, no outflows from the structural source pool occurs during that time step. If there is sufficient N to

satisfy the S_{n1} flow, S_{n2} is then computed as the lesser of (1) the amount needed to maintain microbe pool C:N at 10, or (2) the difference between N available in the source pool and S_{n1}. Last, if there is sufficient N available in the source pool to satisfy both the S_{n1} and S_{n2} flows, S_{n3} is computed as difference between the potential amount of N lost from the source pool (relative to carbon decomposition) and ($S_{n1} + S_{n2}$).

Likewise, for the metabolic leaf and root litter pools, there are two possible N outflow paths; transfer to microbial pools is satisfied first by computing the amount of N needed to maintain the critical C:N of microbe pools. The three possible outflow paths from microbial N pools, and the two possible outflow paths from each soil (SLOW and OLD) N pool are computed according to the same rules and priorities. There is no direct flux from the $SLOW_n$ to the OLD_n pool; transfer is indirect via the soil microbial pool.

Following mineralization calculations, immobilization flow from the MIN_n pool to each litter pool is computed. These flows are dependent on total immobilization demand, which is determined as the sum of all N flows needed to meet the critical C:N ratio of individual litter pools. If total demand exceeds the current MIN_n pool level, each litter pool whose C:N exceeds the critical level receives an equal portion of the MIN_n pool. If total demand is less than the MIN_n level, demand is satisfied completely for each litter pool whose C:N is higher than the critical level. The remaining MIN_n is available for uptake by vegetation.

Impacts of Cultivation on Microbial Respiration

Conversion of native ecosystems to cropping systems through cultivation involves some degree of vegetation clearing, soil tillage and fertilization. We make two modifications for cultivated grid cells. First, plant litter lignin concentrations are set at 5% and the minimum C-to-N ratio of litter is adjusted to 15. Second, turnover rates of soil microbial, SLOW and OLD C pools increase by 25%, 50% and 50%, respectively [Tisdale and Oades, 1982; Parton et al., 1987]. For this model version we assumed that 100% of crop residue is returned to the soil annually with no losses of litter carbon due to harvesting. Future model tests will include nitrogen fertilizer amendments.

Comparison with Other Models

There are several notable differences between the CASA-Biosphere model (this study) and previous ecosystem models with carbon-nitrogen feedbacks that have been applied at regional and global scales, particularly CENTURY [Parton et al., 1987, 1988, and 1989a] and TEM [Raich et al., 1991; McGuire et al., 1992; Melillo et al., 1993]. The major

differences (as summarized in Table 6) include sources and spatial resolutions of climate and vegetation data sets used, the degree to which parameter values are calibrated to specific vegetation types, use of remote sensing observations, and detail of the soil moisture and C/N cycling submodels.

In the TEM, NPP is computed as gross primary productivity (GPP) minus respiration, using atmospheric CO_2 concentrations and solar radiation drivers. It includes unitless scalars for the effects of air temperature, relative N availability, and plant phenology. In this version of the CASA model, we do not compute plant respiration, nor do we consider CO_2 concentrations and N limitation explicitly as controllers of productivity. The TEM equation for N uptake is hyperbolic function of mineral N and temperature, carbon availability, and a biome-specific maximum uptake constant. Other biome-specific parameters in TEM that are not biome-specific in CASA include the timing of litterfall and microbial respiration rates. The TEM uses different climate data sources, vegetation type classification, and a finer spatial resolution (0.5° versus 1.0°).

The CASA soil submodel is based on the CENTURY concept, but has been simplified for global applications. For example, the CASA version does not include optional effects of pH, phosphorus, sulfur, and atmospheric-hydrologic fluxes of nitrogen. CENTURY also includes algorithms for competition between trees and grasses for soil N. Unlike CENTURY, but like TEM, we make no correction for differences between air and soil surface temperature. In the CASA model, the C-to-N ratios of SLOW and OLD soil pools are set according to soil texture [Zobler, 1986], whereas in CENTURY these ratios float over a prescribed range. In both models, N is transferred in proportion to monthly NPP at the amount needed to produce the highest N quality litter possible over a prescribed range.

RESULTS

Net Primary Productivity

The CASA-Biosphere model was applied using global data inputs as described above. On the basis of monthly calculations over 14,713 non-ice terrestrial grid cells, our estimate of total terrestrial net primary production (NPP) is 48 Pg C yr^{-1}. Over 34 Pg C yr^{-1}, or 70% of terrestrial NPP, occurs between 30° N and 30° S latitude, in contrast to 4% at latitudes higher than 60° N and S (Table 7). For individual grid cells, annual NPP ranges from values less than 20 g C m^{-2} in some tundra and desert locations to values greater than 1400 g C m^{-2} in broadleaf evergreen forests of South America and Central Africa (Plate 2).

Approximately one third of all solar radiation impinging on terrestrial surfaces is intercepted by

TABLE 6. Comparisons of Model Attributes

Model	Climate and vegetation	Soil Moisture	NPP and Litterfall	Soil C/N
CASA (this paper)	global 1° data sets, cultivation	1 layer bucket, non-linear drying	function of AVHRR-SR, PAR, moisture and temperature	leaf, root and wood litter, global decay constants, dual microbial/soil pools, soil texture controls on C:N
TEM [Raich et al., 1989; McGuire et al., 1992]	global 0.5° data sets	1 layer bucket, linear drying	GPP minus respiration as a function of PAR, CO$_2$, moisture, and temperature	litter cohorts, single soil pool
CENTURY [Parton et al., 1987; 1988; 1992]	site records, land management	multi layer bucket	climate and soil based regressions	leaf, root, and wood pools, dual microbial/soil pools, floating soil C:N, ecosystem C/N balance

TABLE 7. Annual NPP for Vegetation Classes and Latitude Zones

| Class	Predicted NPP, g C m^{-2} yr^{-1}			Total, Pg C yr^{-1}	%Tot	Latitude Zone Distribution				
						North, deg			South, deg	
	Mean	Max	Stdev			90-60	60-30	30-0	0-30	30-60
1	1027	1463	284	18.0	37	0.00	0.04	7.60	10.29	0.06
2	315	838	148	0.7	2	0.00	0.52	0.11	0.01	0.10
3	316	811	135	1.3	3	0.03	1.08	0.01	0.04	0.14
4	226	819	117	3.6	7	0.73	2.48	0.36	0.00	0.02
5	153	439	72	1.0	2	0.56	0.44	0.00	0.00	0.00
6	559	1206	285	10.4	22	0.01	0.45	2.78	6.96	0.23
7	180	962	175	1.9	4	0.01	0.33	0.70	0.84	0.06
8	469	1065	224	1.1	2	0.00	0.08	0.17	0.67	0.13
9	115	1166	168	1.2	2	0.00	0.24	0.44	0.29	0.19
10	80	522	68	0.5	1	0.39	0.13	0.00	0.01	0.01
11	28	397	34	0.5	1	0.01	0.13	0.20	0.13	0.00
12	288	1074	199	7.8	16	0.01	4.36	1.60	0.80	1.04
Total				48.0	100	1.75	10.28	13.97	20.04	1.98
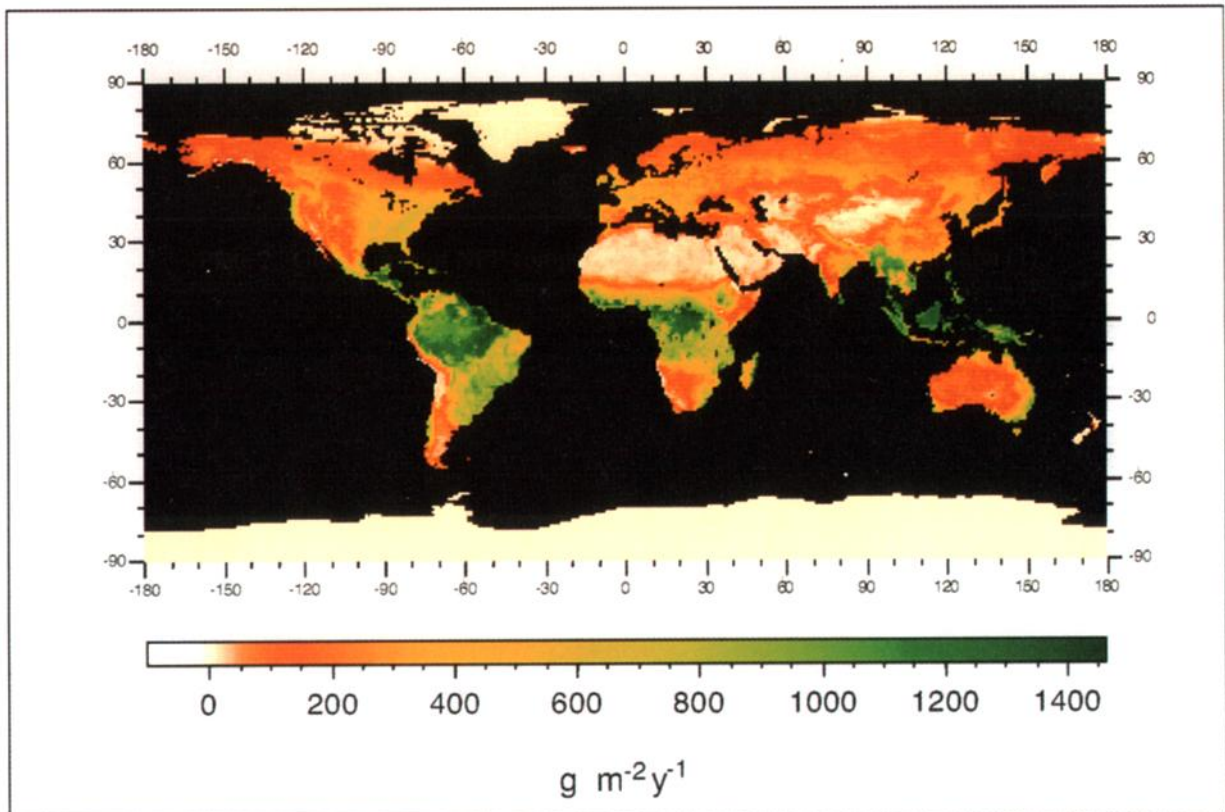
Plate 2. Global map of NPP computed according to the model in equation (1).

plants (Table 8). This fraction varies substantially across ecosystems, with tropical rain forest grid cells intercepting close to 80% and desert grid cells intercepting only about 4%. The total amount of intercepted radiation (1.48×10^{17} MJ PAR yr^{-1}) sets an upper limit to both gross and net primary production.

Applying ε^* to all grid cells (i.e., simply taking the product of 1.48×10^{17} MJ PAR yr^{-1} x 0.39 g C MJ^{-1} PAR) yields a terrestrial NPP of 57 Pg C yr^{-1}. Thus effects of temperature and water stress on our light use efficiency result in a 16% reduction of terrestrial NPP to 48 Pg C yr^{-1}. This relatively small impact of stress on ε reflects both our initial assumptions, which loaded some of water stress variability in NPP into IPAR, and the fact that high efficiencies and high IPAR values tend to co-occur. Note that all stresses on ecosystem production also show up in IPAR (Table 8), and that the sum of stresses on both terms on the right hand side of equation (1) is adjusted in the calibration process (Figure 2). As an example of the co-occurrence of high efficiencies and high IPAR values, broadleaf evergreen forest and broadleaf woodland/savanna ecosystems (classes 1 and 6 in Table 8) on average intercept the most radiation. These ecosystems also have the highest average efficiencies (0.35 and 0.30 g C MJ^{-1} PAR), and contribute the most to the total terrestrial NPP (> 59%).

For other ecosystems, however, water and temperature stress effects on ε are far more severe. The average efficiency for deserts (class 11) is only

35% of ε^*, whereas for shrubs with bare soil (class 9), the average light use efficiency is approximately 54% of ε^*. These two ecosystems comprise a significant fraction of the total land surface area in which growth is constrained by water and temperature stress on the light use efficiency term. Production estimates for these areas are depressed far below what is allowed by ε^*. The overall effect of making ε sensitive to water and temperature stress is to expand the dynamic range of possible NPP estimates consistent with a given distribution of IPAR.

Litterfall Patterns

The seasonal timing of litterfall is latitude dependent (Figure 6). The highest monthly percent litterfall occurs during October between 60° and 65° N. Strong seasonality in litterfall is seen in the northern temperate zone as far south 40° N. Distinct seasonality can be detected in the tropics from 5° to 15° N and from 5° and 20° S.

Seasonal Patterns in NEP

The coupled NPP-soil model was run to a near steady state (< 1% change yr^{-1}) with regard to deviation from zero global NEP (defined as the annual sum of the area-corrected difference between NPP and R_s fluxes). This necessitated approximately 3600 monthly time steps. At the equator, mean NEP (g m^{-2} mo^{-1} over 1° latitude

TABLE 8. Aboveground Model Statistics for Vegetation Classes

Class	S, MJ·10^{15}PAR yr^{-1}	$\Sigma[S*f]$, MJ·10^{15}PAR yr^{-1}	$\Sigma[S*f]/S$	ε, g C MJ^{-1} PAR
1	63.93	49.86	0.780	0.354
2	5.68	2.24	0.388	0.255
3	9.65	4.00	0.411	0.283
4	31.98	11.56	0.359	0.284
5	11.91	3.27	0.269	0.280
6	69.84	30.21	0.438	0.302
7	4.06	6.63	0.168	0.229
8	8.63	3.19	0.376	0.299
9	34.91	4.20	0.119	0.208
10	10.56	1.70	0.160	0.269
11	61.26	2.56	0.042	0.135
12	80.49	25.16	0.324	0.242
Total	440.3	147.6		

Here S is the total annual amount of PAR at the surface, $\Sigma[S*f]$ is the total annual amount of PAR intercepted, and $\Sigma[S*f]/S$ is the fraction of radiation intercepted on an annual basis; ε is the average light use efficiency for months when $T > 0°$ C.
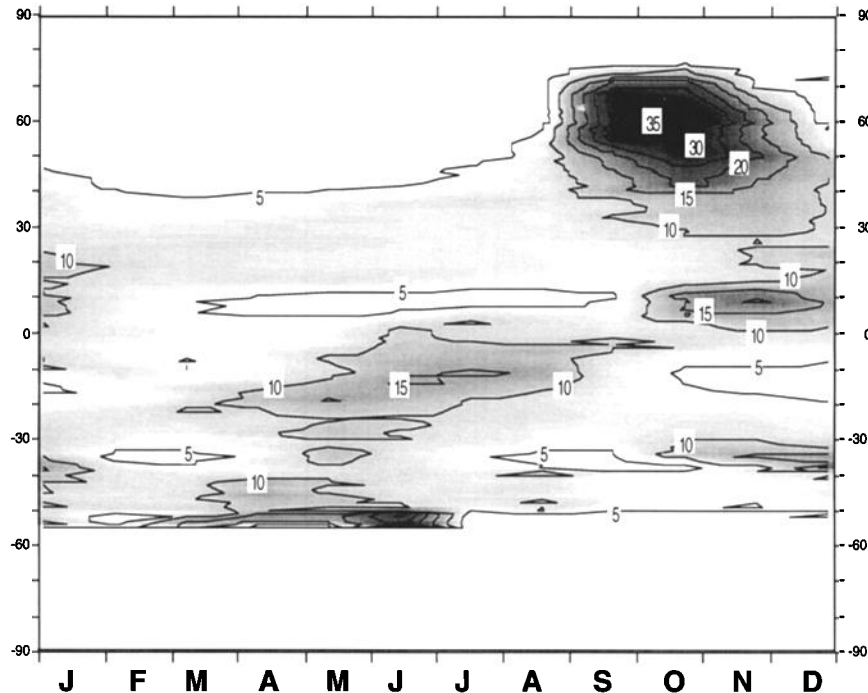
Fig. 6. Seasonal patterns of litterfall over averaged 1° latitude zones. Contour labels are percent of total annual litterfall.

zones) remains constant year-round at less than ±5 g m^{-2} mo^{-1}. In the southern hemisphere tropical zones from 5-23°, NEP is positive from November (nearer the Equator) or December through as late as June at 5° S (Plate 3a). The pattern is reversed in the northern hemisphere tropics, where NEP becomes positive in April (at 5° N) through July-August (for 10-23° N), and turns negative as early as November at the lowest latitudes. In midlatitude zones (40-60° N), NEP is negative from September or October through May, followed by transition to positive with a mean July peak of +25 g m^{-2} (0.032 Pg total) centered around 58° N latitude. At high northern latitudes (above 70° N), NEP turns positive in June and becomes negative throughout the zone by September.

Growing season net flux (GSNF) is defined as the cumulative NEP over the period when NEP is positive. GSNF reflects the magnitude of the net forcing of seasonal variations in atmospheric CO_2 [Fung et al., 1987]. The CASA model estimate of GSNF is largest in forests of the seasonal tropics and the temperate zones (> 120 and > 50 g C m^{-2} growing season^{-1}, respectively; Plate 3b). GSNF is < 40 g C m^{-2} growing season^{-1} for many tropical evergreen forest locations where production and decomposition are relatively aseasonal. The model predicts a global GSNF of 8.8 Pg C. Among the

notable controls on GSNF, the Q_{10} setting for decomposition fluxes (equation (13)) strongly affects seasonal release patterns. Lower values of Q_{10} shift soil microbial sources of CO_2 to spring and fall months; GSNF estimates increase accordingly.

Biome Contributions to Global NEP

For northern hemisphere broadleaf evergreen forests, mean NPP is greater than mean R_s (g m^{-2} mo^{-1} over 1° latitude zones) from September to February (class 1; Figure 7a). In the southern hemisphere, the NEP pattern for the same biome is reversed. Northern midlatitude to high-latitude forests show a positive NEP from June to August (Figure 7b). If these per-unit-area averages are corrected for global area coverage of the biomes, needleleaf evergreen forests (class 4) exchange about six times more carbon than broadleaf deciduous forests (class 2), an observation explained largely by over sevenfold greater area coverage by class 4. Northern grasslands (class 7) and cultivated (class 12) vegetation (Figure 7c) have a low seasonal NEP amplitude relative to temperate forest and northern tundra biome types (class 10; Figure 7d). The lowest seasonal amplitude in NEP is in biomes characterized as bare soil and deserts (class 11), paralleling their small contributions to NPP (Table 7).
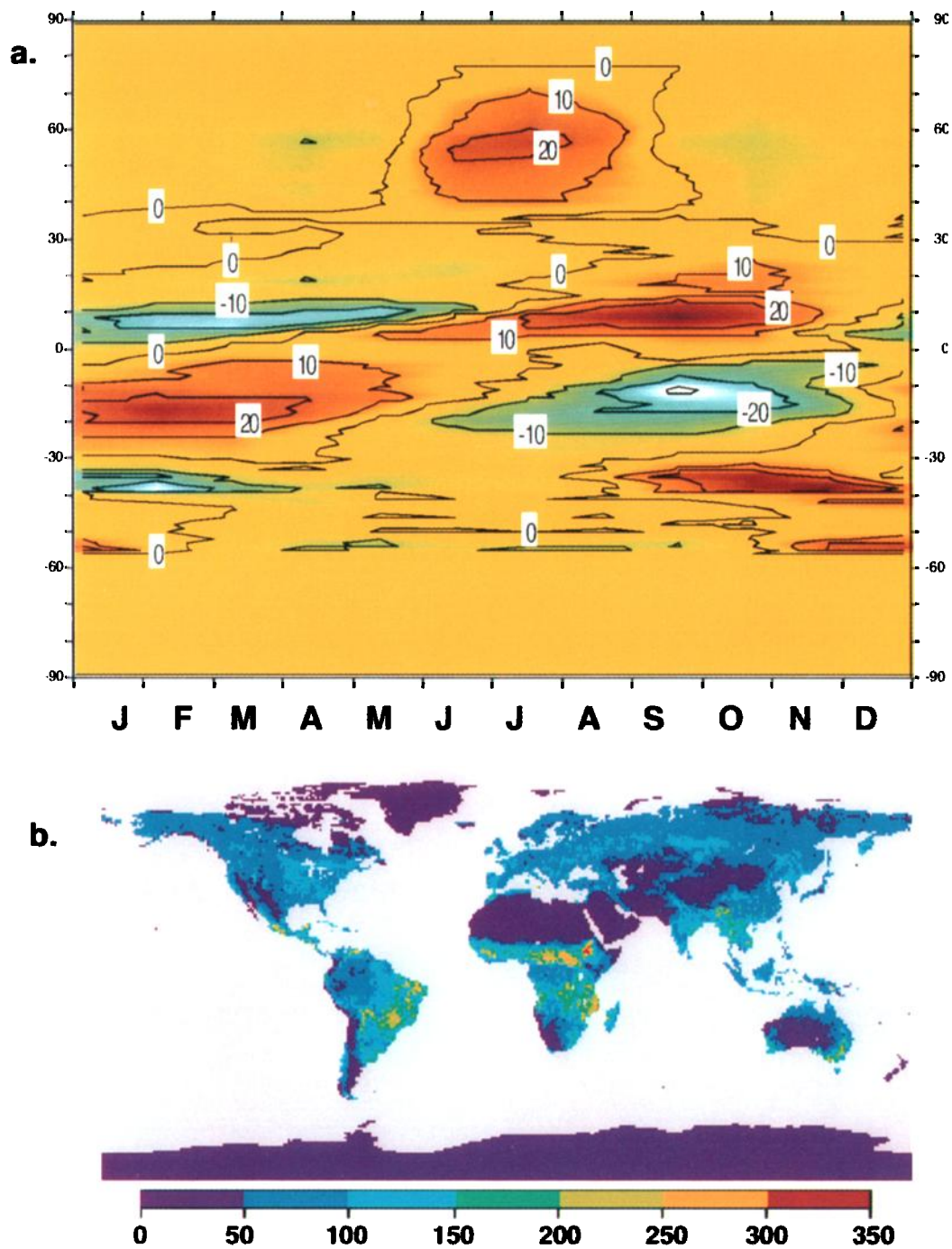
Plate 3. (a) Global NEP averaged over 1° latitude zones. Contour labels are g C m^{-2} mo^{-1}. (b) Growing season net flux (GSNF) in units of g C m^{-2} growing season^{-1}.

Tropical evergreen forests (class 1)

Northern forests (classes 2 and 4)

Northern grassland (class 7) and cultivation (class 12)
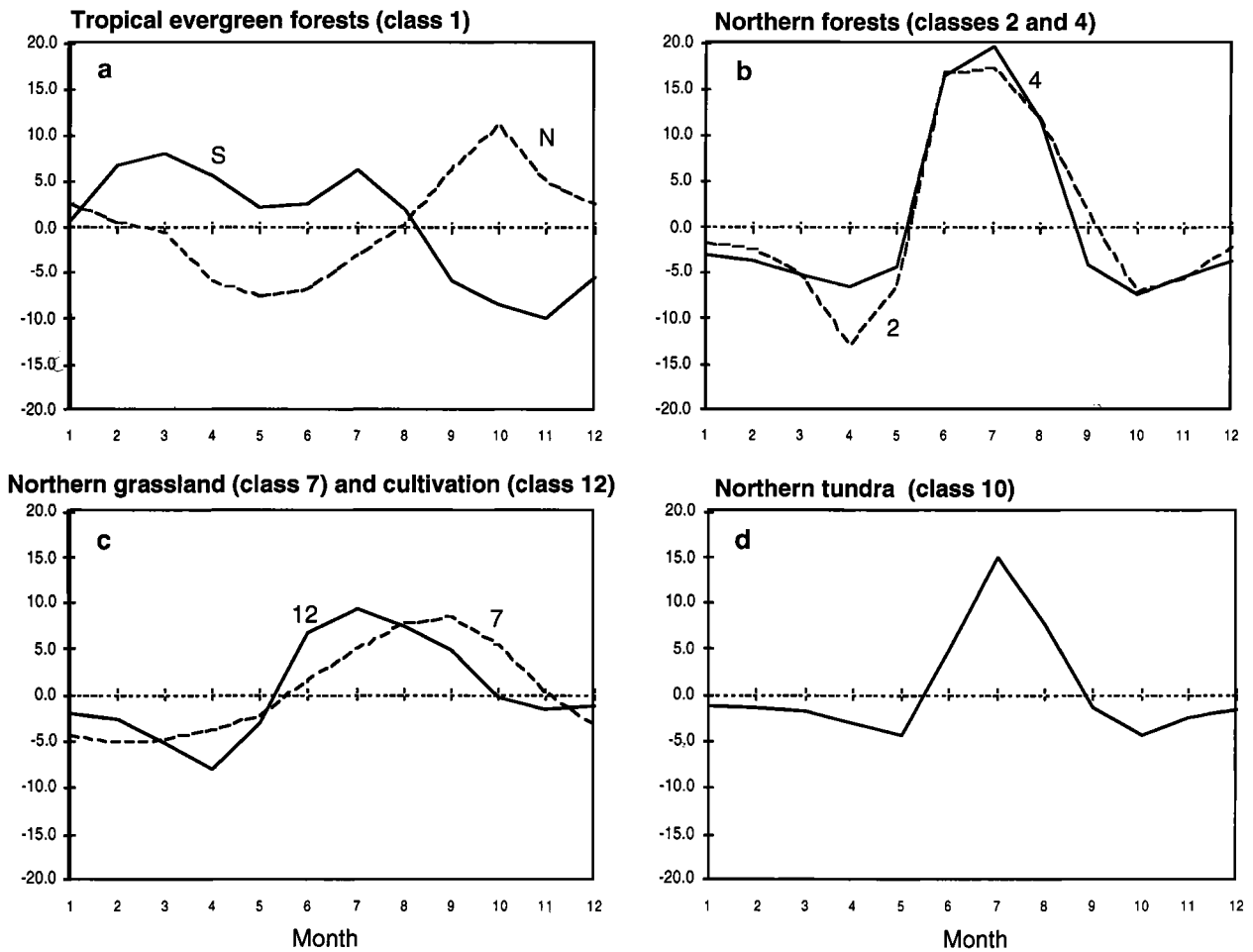
Northern tundra (class 10)

Month

Month

Fig. 7. Seasonality in mean NEP (g C m^{-2} mo^{-1}) by vegetation classes.

Litter and Soil Carbon Pools

Steady state pools of standing litter represent global storage of around 174 Pg C (94 and 80 Pg C in nonwoody and woody pools, respectively; Table 9), whereas storage in the SLOW pool is 300 Pg C. Leaf and fine root litter pools comprise around 51 and 43 Pg C, respectively. The distribution of stored C in litter and soil carbon pools varies with latitude (Figure 8). Two latitude zones, one high-to-mid (70°-30° N) and the other tropical (10° N-30° S), comprise major pools of stored soil carbon. Low levels of total soil C storage in the 15°-40° N zone reflect ecosystem types and processes, rather than latitudinal patterns in land surface area. Storage of carbon in microbial biomass, expressed as a percentage of total soil C, increases from about 4% in high latitudes (> 60° N) to 6% near the Equator. The fraction of soil C in the top 0.3 m made up by the SLOW pool is around 65% at latitudes higher than 30° N, but rises to 70-83% throughout the tropics.

Litter and soil carbon pools (g C m^{-2}) are greatest in mixed temperate forests (class 3, Table 9). Perennial grasslands (class 7) and deserts (class 11), have the lowest litter pools, both per unit area and integrated over area (Table 9).

Turnover times of four litter-soil carbon pools (expressed as the steady state pool size divided by the sum of annual losses) are fastest for biomes found chiefly in the tropics (broadleaf evergreen forests and savanna vegetation classes) and for cultivated areas (Table 10). Carbon turnover in needleleaf deciduous forests and tundra is slowest.

DISCUSSION

Correlations with Atmospheric CO$_2$

As a consistency check of CASA-Biosphere model predictions, we compared our monthly NEP estimates to average atmospheric CO$_2$ concentrations from three stations in the NOAA/Geophysical Monitoring for Climate Change (GMCC) Flask

TABLE 9. Litter and Soil Carbon Pools

Class	Nonwoody[a] Mean, g C m^{-2}	Nonwoody[a] Total, Pg C	Woody Mean, g C m^{-2}	Woody Total, Pg C	Upper soil[b] Mean, g C m^{-2}	Upper soil[b] Total, Pg C
1	1246	21.7	1216	21.2	5291	91.9
2	1196	2.6	1135	2.5	5465	11.8
3	1345	5.3	1290	5.1	5933	23.4
4	1203	18.0	1158	17.3	5645	83.9
5	1195	7.5	1211	7.6	5635	35.3
6	869	15.5	853	15.2	3742	66.5
7	323	3.2	0	0.0	1895	18.8
8	1018	2.3	954	2.1	3915	8.7
9	274	2.7	260	2.5	1468	13.9
10	787	5.0	758	4.7	3447	21.8
11	74	1.1	146	2.2	718	10.5
12	333	8.8	0	0.0	2335	58.9
Total		93.7		80.4		445.4

[a]Includes leaves and fine roots.
[b]In top 0.3 m of profile.
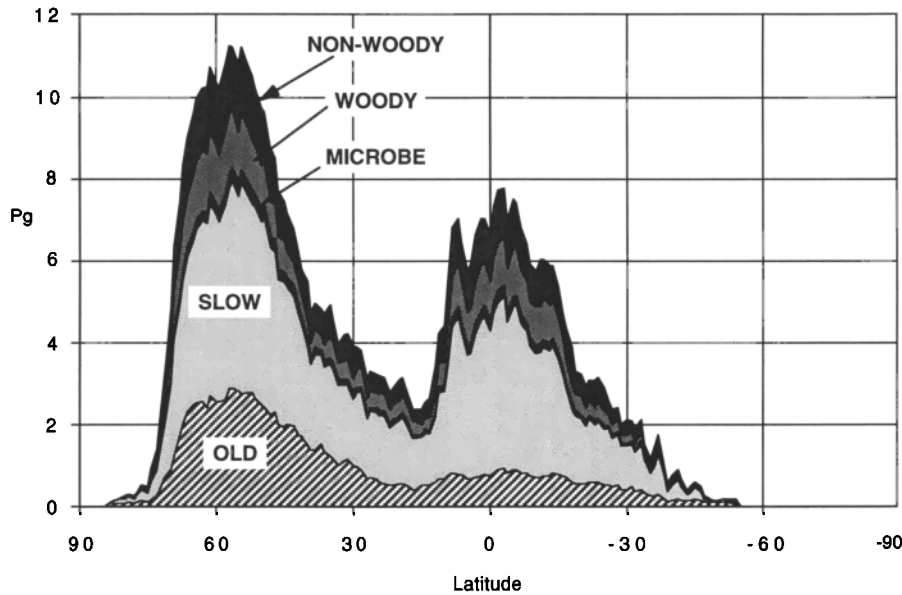

Fig. 8. Latitude-based litter and soil carbon pool totals (Pg C).

Sampling Network during 1986 [Conway and Tans, 1989]. Although the atmospheric CO_2 concentration is an integrated response to terrestrial and oceanic processes, combined with the effects of anthropogenic fossil fuel and land use sources, terrestrial carbon fluxes dominate the seasonal signal [Fung et al., 1987]. Monthly changes in CO_2 concentrations (dCO_2) are roughly mirror images of

zonally averaged NEP (Figures 9a-9c). We used CO_2 measurements from Point Barrow, Alaska (BRW) at 71° N, Mauna Loa, Hawaii (MLO) at 20° N, and Christmas Island (CHR) at 2° N for comparisons to monthly NEP averaged over 50°-80° N, 10°-30° N, and 0°-10° N respectively. The latitude zones for BRW and MLO were the same as those used by Tucker et al. [1986] for a similar

TABLE 10. Turnover Times for Carbon in Four
Litter/Soil Pools Shown in Figure 5

	Carbon Pool Turnover Time, yr			
Class	ML	SM	SLOW	OLD
1	0.2	0.6	9	264
2	0.9	1.6	28	815
3	1.1	1.7	32	936
4	1.3	2.1	40	1177
5	1.9	3.3	64	1873
6	0.3	0.8	13	393
7	0.6	1.2	23	679
8	0.4	0.9	16	483
9	0.5	1.1	21	611
10	1.9	4.2	84	2466
11	0.7	2.0	39	1162
12	0.7	1.1	15	457

Metabolic Litter (ML), Soil Microbes (SM),
SLOW, and OLD organic matter.

analysis. For all three station locations, positive
dCO_2 values were associated with transitions to
consistently negative NEP, which indicates net
carbon losses from terrestrial ecosystems through
microbial respiration. Negative dCO_2 values were
accompanied by increases in NEP to comparatively
high and consistently positive values that would
indicate net ecosystem carbon gains through
photosynthetic fixation.

Simple linear regression of the paired monthly
dCO_2 concentrations versus NEP estimates resulted
in negative slopes and r^2 values of 0.67, 0.09, and
0.24 for BRW, MLO, and CHR, respectively. If a
one month lag was assumed (to account for
atmospheric mixing), so that NEP for month t is
plotted against dCO_2 for month $t+1$, the coefficients
become 0.19 for BRW, 0.52 for MLO, and 0.17 for
CHR. Atmospheric circulation and boundary-level
mixing effect may cause a delay of about a month in
equilibrium CO_2 concentrations at MLO, which is
thought to be characteristic of globally averaged CO_2
cycle [Tucker et al., 1986].

Model Result Comparisons of Production

The terrestrial production estimate from the
CASA-Biosphere model of 48 Pg C yr^{-1} is within
several Pg C of previously published estimates. For
example, the TEM estimate is 53.2 Pg C yr^{-1} [Melillo
et al., 1993]. Although we use the some of the same
calibration sites as those used in TEM for our NPP
estimates, the modeling approaches are sufficiently
different that continental estimates are only loosely
constrained. On a continental basis, our model
estimates production for North and South America at
6.1 and 14.4 Pg C yr^{-1}, respectively, compared to

TEM predictions of 7.0 [McGuire et al., 1992] and
12.5 Pg C yr^{-1} [Raich et al., 1991]. The average
CASA-Biosphere model estimate for NPP (g m^{-2}
yr^{-1}) in tropical evergreen forests is about 6% higher
than the corresponding TEM prediction, which may
explain the difference in total production for the
South American continent. Differences in area
estimates for the various vegetation types, however,
confound this analysis.

We compared grid cell estimates of NPP from the
CASA-Biosphere and MIAMI [Lieth, 1975] models.
Figure 10 shows these estimates aggregated for
vegetation types. The MIAMI model estimates
global terrestrial NPP at around 61 Pg C, which is
about 20% higher than the CASA model prediction.
The lower CASA NPP estimates for many biomes
may be due in part to the sensitivity of our model to
IPAR. Even though the mean climate - NPP
regressions developed in the MIAMI model may
suggest a potential NPP for a grid cell, there can be
areas within the cell where plants do not persist
(e.g., surface area covered by rock, lakes or asphalt)
or times of the year when human management has
altered the land cover. These bare areas will lower
the average IPAR for the grid cell and thus reduce the
average NPP calculated in CASA for the biome type
on a per square meter basis. For example, the CASA
predicted NPP for class 11 (bare soil and deserts) is
less than one third of the MIAMI model estimate.

Implications for Litter and Soil C Storage

The CASA-Biosphere model predicts that
undecomposed litter plus carbon pools in the upper
(0.3 m) soil contain about 620 Pg C, slightly more
than one-third of Schlesinger's [1991] global
estimate of 1500 Pg C which considers soil pools to
1.0 m depth. Our prediction of nonwoody surface
litter (51 Pg C) is close to Schlesinger's [1977]
estimate of 55 Pg C. The CASA prediction for
standing litter pools in the tropics is somewhat higher
than expected, compared to those for temperate
forests (Table 9). One reason for this pattern is that
overall litter decomposition rates can be
underestimated using the fractionation algorithm
shown in equation (16) [Parton et al., 1993],
especially if the litter lignin-to-nitrogen ratio is high.

Model results (not shown here) indicate that C-to-
N ratios of litter entering the soil system consistently
tend toward minimum levels for all vegetation
classes, except in extreme high-latitude areas. Under
the present model structure, N mineralization rates
are adequate to meet the maximum demands of
vegetation. This pattern may result from sensitivity
to the initial state of soil N pools, which follow from
a spatially uniform fraction of Post et al.'s [1985]
storage estimates. The overall availability of nitrogen
to plant, litter, microbe and soil pools is fixed to
these initial levels. Further tests involving soil N
initialization levels and feedbacks on decomposition
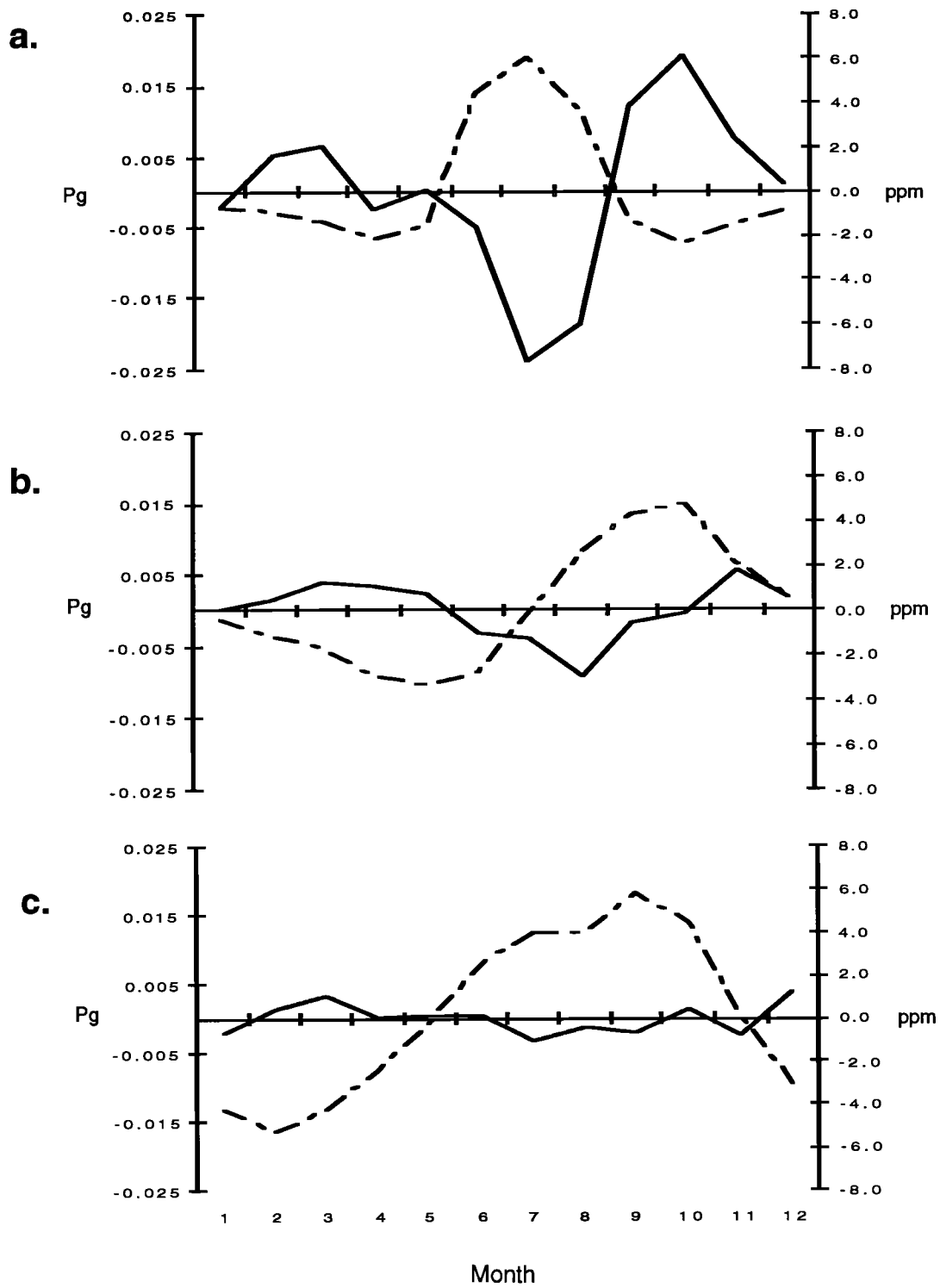rates are underway to better understand ecosystem

Fig. 9.   Comparisons of atmospheric dCO_2 concentrations (solid lines) and NEP (dashed lines) for (a) Point Barrow, Alaska (BRW), (b) Mauna Loa, Hawaii (MLO), and (c) Christmas Island (CHR).
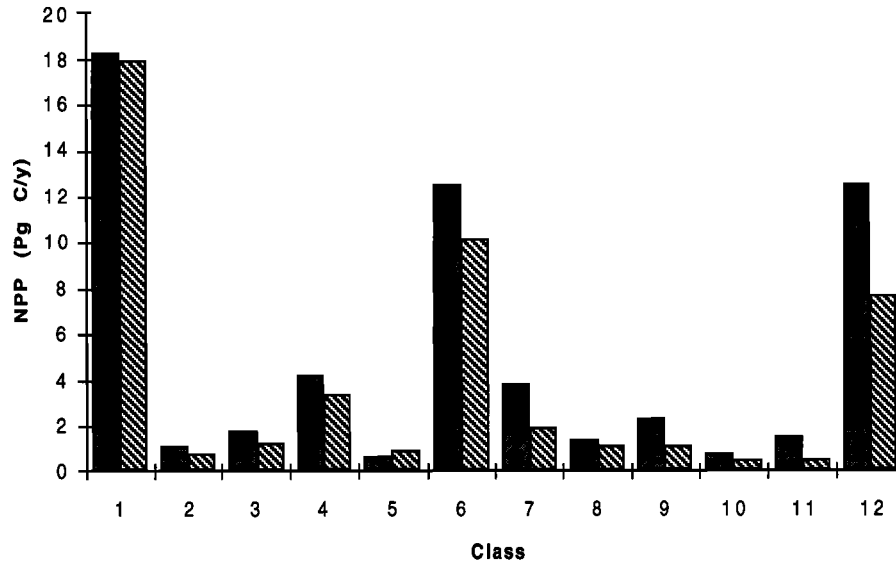
Fig. 10. Comparison of model NPP model predictions by vegetation classes from Dorman and Sellers [1989]. Shaded bars are MIAMI model [Lieth, 1975] predictions; hatched bars are CASA model (this study) predictions.

model sensitivity to nitrogen sources and sinks.

Comparison of our steady state estimates of soil carbon pools to initial model conditions, the latter of which matches the geographic distribution for life zones as reported by Post et al. [1985], indicates that the simulation predicts somewhat lower soil carbon storage at high latitudes to mid latitudes ($90°-30°$ N) and higher pools in tropical ($20°$ N-$20°$ S) latitudes. Part of the difference may be due to the fact that we model only the upper 0.3 m of the soil, while Post et al. [1985] consider C storage to 1 m soil depth. However, if we compare the average CASA model estimate of carbon stored in upper soil layers of moist tropical forests (5.3 kg m^{-2} to 0.3 m depth) to Detwiler's [1986] estimate of 6.5 kg m^{-2} to 0.4 m depth, there is closer correspondence between observed and predicted. It should be noted, however, that the distribution of C storage in upper soil layers does not necessarily reflect soil carbon pools below 0.3 m depth. Previous comparisons suggest that the greatest difference between tropical and temperate soils is found in deep profile layers [Sanchez et al., 1982]. Our focus on the top 0.3 m soil is attributed to poor understanding of organic matter dynamics in deeper soils.

Another explanation for the prediction of relatively large soil C pools in the tropics is that 66% of all fine textured soils in the FAO-SMW are located between $30°$ N and $30°$ S [Zobler, 1986]; as pointed out by Parton et al. [1989b], the model structure used in CASA reduces the fraction of carbon lost as CO_2 during transfer to the SLOW pool in tropical soils with high silt-clay contents as per equation (18). In addition, CASA overlooks the effect of seasonal fires on reduction of soil organic matter accumulation, which may be particularly important in dry tropical areas.

The fraction of total soil carbon made up by the SLOW soil pool, which we estimate to have a residence time of 10-85 yr in most upper soil layers (Table 10), has important implications for studies of the global carbon cycle. We estimate that this fraction makes up around 65% of carbon in soil upper layers at latitudes higher than $30°$ N, but is as high as 83% in tropical zones. The model predicts a global SLOW pool of 300 Pg C in the surface (0.3 m) soil layers, which represents less than one third of estimated global litter and soil C storage [Houghton et al., 1990; Schlesinger, 1991]. Independent estimates using soil radiocarbon measurements of SLOW C pool size and turnover time by Harrison et al. [1993] suggested values somewhat higher than our own (75% of the total with turnover time of 25 yr, for a SLOW pool total of about 500 Pg C). Results from the CASA-Biosphere model suggest that, under a climate warming scenario, higher turnover times of relatively large SLOW carbon pools in tropical ecosystems may lead to substantial increases in CO_2 fluxes from microbial respiration, as predicted by a simpler model [Townsend et al., 1992].

Advantages and Limitations of the Model

The CASA experience shows that remote sensing and GIS technologies, when used in conjunction with large scale land data bases, can help bridge the gap in scales that exists between global biosphere models and the very local data used to calibrate them. Nevertheless, the NPP calibration process used in CASA has scaling limitations of both a temporal and spatial nature. Predictions are based on mean monthly climate data from the period 1930-1960 and remote sensing observations collected from a single

year (1987). In the calibration process, predicted NPP is compared with observations that have been gathered at various intervals over the past 30 years. The temporal discontinuity between climate, satellite and NPP site observations introduces uncertainty into CASA model estimates. Such discontinuities may be reduced in part as more satellite data become available for use in multi-year global biosphere studies. Uncertainty is also introduced into the model as a result of the difference in spatial resolution between climate/satellite data sets (~100 km) and NPP site data (with plot sizes ranging from meters to hundreds of meters). The main difficulty is that calibration sites cannot represent the heterogeneity within 1° grid cells. Features such as lakes, bare soil, and asphalt act to reduce satellite derived vegetation indices. We expect that, in general, per area regional estimates of NPP to be somewhat less than the values observed at small study sites, but the magnitude of this effect is difficult to determine without studies based on finer scale data.

Another set of limitations involves the use of a single layer soil submodel for moisture controls. First, element leaching to layers below the rooting zone was not considered in this study. Second, while the soil submodel integrates moisture availability over the top 1-2 m of soil, the scalar used to calculate carbon turnover and nitrogen mineralization fluxes applies only to the upper 0.3 m of the soil profile. Third, a single layer soil model fails to adequately account for the high efficiency with which a dry upper layer prevents evaporative loss from wetter lower layers [Hillel, 1980].

The confidence one places in model predictions depends to a large degree on reliability of input data sets. Modeling at the global scale currently necessitates use of data inputs that have not been extensively verified. This is particularly true for land use and soil data sets, where the problems involve both the density of measured sites and the consequences of aggregation to a few classes.

Models based on remote sensing data have relatively strong potential to analyze temporal changes during the era of satellite data, but their applicability to other times, climates, and biome distributions is less clear. Without additional algorithms for simulating changes in NDVI under

altered conditions, the CASA-Biosphere model has limited use for climate- or vegetation-change scenarios. Extensions and improvements in the satellite record will enhance its usefulness for detecting and quantifying global change.

CONCLUDING REMARKS

The CASA-Biosphere model links ecological regularity (e.g., the IPAR:NPP relationship) and process-level descriptions (e.g., effects of temperature and water on NPP and soil C and N transformations) with satellite and surface data at the global scale. The result has some limitations, but also some unique advantages. The use of an AVHRR-based vegetation index gives the model rich access to intra-annual and interannual variability, including some aspects of agriculture and land use change. Because the model emphasizes scaling at the process rather than the biome level, the results are only sparingly sensitive to the quality and quantity of data characterizing any single ecosystem type. This approach also tends to minimize impacts of structural and taxonomic variation within regions classified as a single biome.

Modeled global NPP is comparable to estimates from other recent models, and the seasonal pattern of modeled global NEP is consistent with the intra-annual dynamics of atmospheric CO_2. Improved validation will depend on finer scale remote sensing data and on new experimental data, concerning both ecosystem processes and the spatial and temporal distribution of atmospheric CO_2.

While the CASA approach is not ideally suited for studies of land use, atmospheric, and climate change, its can contribute to efforts along those lines. The generation of models that successfully simulates response(s) of the terrestrial biosphere to changes in land use, atmospheric CO_2, and climate will be likely to include components from diverse approaches.

APPENDIX

Major pool variables and scalars are described in this appendix. Variable definition sources include data input drivers (D), spatially uniform settings (U), and model calculations (M).

TABLE A1. Definitions for Major Pool Variables and Scalars

Name	Description	Source	Value	Units
	Soil Moisture Submodel			
EET	Estimated evapotranspiration	M		m mo^{-1}
PACK	Snow pack pool	M		m
PET	Potential evapotranspiration	M		m mo^{-1}

TABLE A1. (continued)

Name	Description	Source	Value	Units
PPT	Precipitation	D		m mo^{-1}
RDR	Relative drying rate scalar	M	0-1	unitless
SOILM	Soil moisture storage pool	M		m
T	Air temperature	D		°C

NPP and Litterfall Submodel

Name	Description	Source	Value	Units
ε	Light utilization efficiency	M		g C MJ^{-1} PAR
IPAR	Intercepted PAR	M		MJ
LT$_{LAI}$	Monthly litterfall fraction	M	0-1	unitless
NPP	Net primary productivity	M		g C m^{-2} mo^{-1}
PAR	Photosynthetically active radiation	M		MJ mo^{-1}
SOL	Solar radiation	D		MJ mo^{-1}
T$_{opt}$	Temperature optimum for NPP	M		°C
T$_{\varepsilon 1}$	Temperature stress factor	M	0-1	unitless
T$_{\varepsilon 2}$	Temperature stress factor	M	0-1	unitless
W$_{\varepsilon}$	Water stress factor	M	0-1	unitless

Soil C/N Submodel

Name	Description	Source	Value	Units
ETX	Soil texture effect scalar	M	0-1	unitless
LFA$_c$	Leaf carbon allocation fraction	U	0.33	unitless
LF$_l$	Leaf lignin fraction	M	0-1	unitless
LM$_c$	Surface litter microbial C pool	M		g C m^{-2}
LM$_{cn}$	Surface litter microbial C-to-N ratio	U	10	unitless
LM$_k$	Surface litter turnover rate	U	0.455	mo^{-1}
LM$_n$	Surface litter microbial N pool	M		g N m^{-2}
M$_\varepsilon$	Microbial C assimilation efficiency	U	0.45	unitless
MIN$_n$	Mineral nitrogen pool	M		g N m^{-2}
ML$_c$	Metabolic leaf litter carbon pool	M		g C m^{-2}
ML$_{cn}$	Metabolic leaf litter C-to-N ratio	U	25	unitless
ML$_k$	Metabolic leaf litter turnover rate	U	0.703	mo^{-1}
ML$_n$	Metabolic leaf litter nitrogen pool	M		g N m^{-2}
MR$_c$	Metabolic root litter carbon pool	M		g C m^{-2}
MR$_{cn}$	Metabolic root litter M-to-N ratio	U	25	unitless
MR$_k$	Metabolic root litter turnover rate	U	0.781	mo^{-1}
MR$_n$	Metabolic root litter nitrogen pool	M		g N m^{-2}
OLD$_c$	Old soil carbon pool	M		g C m^{-2}
OLD$_k$	Old soil carbon turnover rate	U	0.00056	mo^{-1}
OLD$_n$	Old soil nitrogen pool	M		g N m^{-2}
Q$_{10}$	Q$_{10}$ constant	U	2.0	unitless
RTA$_c$	Root carbon allocation fraction	U	0.33	unitless
RT$_l$	Root lignin fraction	M	0-1	unitless
SL$_c$	Structural leaf litter carbon pool	M		g C m^{-2}
SL$_{cn}$	Structural leaf/root C-to-N ratio	M	150	unitless
SL$_n$	Structural leaf litter nitrogen pool	M		g N m^{-2}
SLOW$_c$	Slow soil carbon pool	M		g C m^{-2}
SLOW$_k$	Slow soil carbon turnover rate	U	0.0163	mo^{-1}
SLOW$_n$	Slow soil nitrogen pool	M		g N m^{-2}
SM$_c$	Soil microbial carbon pool	M		g C m^{-2}
SM$_{cn}$	Soil microbial C-to-N ratio	U	10	unitless

TABLE A1. (continued)

Name	Description	Source	Value	Units
SM_n	Soil microbial nitrogen pool	M		$g\ N\ m^{-2}$
SRT_c	Structural root litter carbon pool	M		$g\ C\ m^{-2}$
SRT_n	Structural root litter nitrogen pool	M		$g\ N\ m^{-2}$
T_s	Soil temperature effect scalar	M	0-2.8	unitless
WDA_c	Woody carbon allocation fraction	U	0.33	unitless
WD_c	Woody detritus carbon pool	M		$g\ C\ m^{-2}$
WD_{cn}	Woody detritus C-to-N ratio	U	260	unitless
WD_k	Woody detritus carbon turnover rate	U	0.04	mo^{-1}
WD_l	Woody detritus lignocellulose fraction	M	0.35	unitless
WD_n	Woody detritus nitrogen pool	M		$g\ N\ m^{-2}$
W_s	Soil water effect scalar	M	0-1	unitless

REFERENCES

Ajtay, G. L., P. Ketner, and P. Duvigneaud, Terrestrial primary production and phytomass, in *The Global Carbon Cycle*, edited by B. Bolin et al., pp. 129-181, John Wiley, New York, England, 1979.

Amthor, J. S., *Respiration and Crop Productivity*, Springer-Verlag, New York, 1989.

Anderson, D. W., S. Saggar, J. R. Bettany, and J. W. B. Stewart, Particle size fractions and their use in studies of soil organic matter, I, The nature and distribution of forms of carbon, nitrogen, and sulfur, *Soil Sci. Soc. Am. J.*, 45, 767-772, 1981.

Anderson, J. M., The effects of climate change on decomposition processes in grassland and coniferous forests, *Ecol. Appl.*, 1(3), 326-347, 1991.

Bacastow, R. B., C. D. Keeling, and T. P. Whorf, Seasonal amplitude increase in atmospheric CO_2 concentration at Mauna Loa, Hawaii, 1959-1982, *J. Geophys. Res.*, 90, 10,529-10,540, 1985.

Berg, B., and H. Staff, Leaching, accumulation and release of nitrogen in decomposing forest litter, in Terrestrial Nitrogen Cycles, edited by F. E. Clark and T. Rosswall, *Ecol. Bull.*, 33, 163-178, 1981.

Berry, J., and O. Björkman, Photosynthetic response and adaptation to temperature in higher plants, *Ann. Rev. Plant Physiol.*, 31, 491-543, 1980.

Bishop, J. K. B., and W. B. Rossow, Spatial and temporal variability of global surface solar irradiance, *J. Geophys. Res.*, 96, 16,839-16,858, 1991.

Bouwman, L. A. F., I. Fung, E. Matthews, and J. John, Global analysis of the potential for N_2O production in natural soils, *Global Biogeochem. Cycles*, 7, 557-597, 1993.

Box, E., B. N. Holben, and V. Kalb, Accuracy of AVHHR vegetation index as a predictor of biomass, primary productivity and net CO_2 flux, *Vegetatio*, 80, 71-89, 1989.

Cameron, R. S., and A. M. Posner, Mineralisable organic nitrogen in soil fractionated according to particle size, *J. Soil Sci.*, 30, 565-577, 1979.

Chapin, F. S., III, The mineral nutrition of wild plants, *Ann. Rev. Ecol. and Syst.*, 11, 233-260, 1980.

Chew, R. M. and A. E. Chew, Primary Productivity of a desert shrub community, *Ecol. Monogr.*, 35, 355-375, 1965.

Chichester, F. W., Nitrogen in soil organo-mineral sedimentation fractions, *Soil Sci.*, 107(5), 356-363, 1969.

Choudhury, B.J., Relationships between vegetation indices, radiation absorption, and net photosynthesis evaluated by a sensitivity analysis, *Remote Sens. Environ., 22,* 209-233, 1987.

Cole, D. W., and M. Rapp, Element cycling in forest ecosystems, in *Dynamic Properties of Forest Ecosystems,* edited by D. E. Reichle, pp. 341-409, Cambridge University Press, New York, 1981.

Conway, T. J., and P. P. Tans, Atmospheric CO_2 Concentrations - The NOAA/Geophysical Monitoring for Climate Change (GMCC) Flask Sampling Network, Rep. NDP-005/R1, Carbon Dioxide Info. and Anal. Cent., Oak Ridge Nat. Lab., U.S. Dep. of Energy, Oak Ridge, Tenn, 1989.

Coupland, R. T., and G. M. Van Dyne, Natural temperate grasslands: Systems synthesis, in *Grassland Ecosystems of the World: Analysis of Grasslands and their Uses,* IBP 18, edited by R. T. Coupland, pp. 97-106, Cambridge University Press, New York, 1979.

DeAngelis, D. L., R. H. Gardner, and H. H. Shugart, Productivity of forest ecosystems studied during the IBP: The woodlands data set, in *Dynamic properties of forest ecosystems,* edited by D. E. Reichle, pp. 567-672, Cambridge University Press, New York, 1981.

Demetriades-Shah, T. H., E. T. Kanemasu, I. D. Flitcroft, and H. Su, Comparison of ground- and satellite-based measurements of the fraction of photosynthetically active radiation intercepted by tallgrass prairie, *J. Geophys. Res., 97,* 18,947-18,950, 1992a.

Demetriades-Shah, T. H., M. Fuchs, E. T. Kanemasu, and I. Flitcroft, A note of caution concerning the relationship between cumulated intercepted solar radiation and crop growth, *Agric. For. Meteorol., 58,* 193-207, 1992b.

Detwiler, R. P., Land use change and the global carbon cycle: The role of tropical soils, *Biogeochemistry, 2,* 67-93, 1986.

Dorman, J. L., and P. J. Sellers, A global climatology of albedo, roughness length and stomatal resistance for Atmospheric General Circulation Models as represented by the Simple Biosphere Model (SiB), *J. Appli. Meteorol., 28,* 833-855, 1989.

Ehleringer, J., and O. Björkman, Quantum yields for CO_2 uptake in C3 and C4 plants, *Plant Physiol., 59,* 86-90, 1977.

FAO/UNESCO, *Soil Map of the World.* 1:5,000,000, Food and Agriculture Organization, United Nations Educational, Scientific, and Cultural Organization, Paris, 1971.

Field, C. B, Ecological scaling of carbon gain to stress and resource availability, in *Integrated Responses of Plants to Stress,* edited by H. A. Mooney et al., pp. 35-65, Academic, San Diego, Calif., 1991.

Friedlingstein, P., C. Delire, J. F. Müller, and J. C.

Gérard, The climate induced variation of the continental biosphere: A model simulation of the last glacial maximum, *Geophys. Res. Lett., 19*(9), 897-900, 1992.

Fung, I. Y., C. J. Tucker, and K. C. Prentice, Application of advanced very high resolution radiometer vegetation index to study of atmosphere-biosphere exchange of CO_2, *J. Geophys. Res., 92,* 2999-3015, 1987.

Garcia, R., E. T. Kanemasu, B. L. Blad, A. Bauer, J. L. Hatfield, D. J. Major, R. J. Reginato, and K. G. Hubbard, Interception and use efficiency of light in winter wheat under different nitrogen regimes, *Agri. For. Meteorol., 44,* 175-186, 1988.

Gardiner, M. J., Use of retrieval and global soils data for global climate modeling, in *Land Surface Processes in Atmospheric General Circulation Models,* edited by P. S. Eagleton, Cambridge University Press, New York, 1982.

Gosz, J. R., Nitrogen cycling in coniferous ecosystems, in Terrestrial Nitrogen Cycles, edited by F. E. Clark and T. Rosswall, *Ecol. Bull., 33,* 405-426, 1981.

Goward, S. N., C. J. Tucker, and D. G. Dye, North American vegetation patterns observed with the NOAA-7 advanced very high resolution radiometer, *Vegetatio, 64,* 3-14, 1985.

Gregorich, E. G., R. P. Voroney, and R. G. Kachanoski, Turnover of carbon through the microbial biomass in soils with different textures, *Soil Biol. Biochem., 23*(8), 799-805, 1991.

Grime, J. P., *Plant Strategies and Vegetation Processes,* John Wiley, New York, 1979.

Harmon, M. E., J. F. Franklin, and F. J. Swanson, Ecology of coarse woody debris in temperate ecosystems, *Adv. Ecol. Res., 15,* 133-302, 1986.

Harrison, K., W. Broecker, and G. Bonani, A strategy for estimating the impact of CO_2 fertilization of soil carbon storage, *Global Biogeochem. Cycles, 7*(1), 69-80, 1993.

Heal, O. W, P. W. Flanagan, D. D. French, and S. F. Maclean, Jr., Decomposition and accumulation of organic matter, in *Tundra Ecosystems: A Comparative Analysis,* IBP Programme 25, edited by L. C. Bliss et al., pp. 587-632, Cambridge University Press, New York, 1981.

Heimann, M., and C. D. Keeling, A three dimensional model of atmospheric CO_2 transport based on observed winds, II, Model Description, in *Aspects of Climate Variability in the Pacific and Western America,* Geophys. Monogr. Ser. vol. 55, edited by D. H. Peterson, pp. 240-260, AGU, Washington, D. C., 1989.

Hillel, D., *Applications of Soil Physics,* 390 pp., Academic, San Diego, Calif., 1980.

Hinds, A. A., and L. E. Lowe, Distribution of carbon, nitrogen, sulphur and phosphorus in particle-size separates from gleysolic soils, *Can. J. Soil Sci., 60,* 783-786, 1980.

Holdridge, L. R, *Life Zone Ecology,* 206 pp,

Tropical Science Center, San Jose, Costa Rica, 1967.

Holmes, R. M., Estimation of soil moisture content using evaporation data, in *Proceedings of Hydrology Symposium*, No. 2, Canadian National Research Council, 1961.

Houghton, R. A., Biotic changes consistent with the increased seasonal amplitude of atmospheric CO_2 concentrations, *J. Geophys. Res.*, *92*, 4223-4230, 1987.

Houghton, J. T., G. T. Jenkins and J. J. Ephraums (Eds.) *Climate Change: The IPCC Scientific Assessment*, 365 pp., Report of the Intergovernmental Panel on Climate Change, Cambridge University Press, New York, 1990.

Houghton, J. T., B. A. Callander, and S. K. Varney (Eds.), *Climate Change 1992: The Supplementary Report to the IPCC Scientific Assessment*, 24 pp., Report of the Intergovernmental Panel on Climate Change, Cambridge University Press, New York, 1992.

Insam, H., D. Parkinson, and K. H. Domsch, Influence of macroclimate on soil microbial biomass, *Soil Biol. Biochem.*, *21*(2), 211-221, 1989.

Jenkinson, D. S., and J. H. Rayner, The turnover of soil organic matter in some of the Rothamsted classical experiments, *Soil Sci.*, *123*, 298-305, 1977.

Kinyamario, J. I., and S. K. Imbamba, Savanna at Nairobi National Park, in *Primary Productivity of Grass Ecosystems of the Tropics and Subtropics*, edited by S. P. Long, M. B. Jones and M. J. Roberts, pp. 25-69, Chapman and Hall, London, 1992.

Kuchler, A. W., World map of natural vegetation, in *Goode's World Atlas*, 16th ed., pp. 16-17, Rand McNally, 1983.

Kumar, M., and J. L. Monteith, Remote sensing of crop growth, in *Plants and the Daylight Spectrum*, edited by H. Smith, pp. 133-144, Academic, San Diego, Calif., 1981.

Ladd, J. H., J. M. Oades, and M. Amato, Microbial biomass formed from [14]C- and ^{15}N-labeled plant material decomposition in soils in the field, *Soil Biol. Biochem.*, *13*, 119-126, 1981.

Leemans, R., Possible changes in natural vegetation patterns due to a global warming, Rep. WP-08, 22 pp., Int. Inst. for Appl. Syst. Anal., Laxenberg, Austria, 1990.

Leemans, R. and W. P. Cramer, The IIASA database for mean monthly values of temperature, precipitation and cloudiness of a global terrestrial grid, Rep. WP-41, 60 pp., Int. Inst. for Appl. Syst. Anal., Laxenberg, Austria, 1990.

Lieth, H., Modeling the primary production of the world, in *Primary Production of the Biosphere*, edited by H. Lieth and R. H. Whittaker, pp. 237-263, Springer-Verlag, New York, 1975.

Los, S. O., C. O. Justice, and C. J. Tucker, A global 1x1 degree NDVI data set for climate studies, *Int. J. Remote Sens.*, in press, 1993.

Matthews, E., Prescription of land-surface boundary conditions in GISS GCM II: A simple method based on high-resolution vegetation data bases, *NASA Tech. Memo.*, *86096*, 20 pp., 1984.

Matthews, E., Atlas of archived vegetation, land-use and seasonal albedo data sets, *NASA Tech. Memo.*, *86199*, 53 pp.,1985.

McCree, K. J., Photosynthetically active radiation, in *Physiological Plant Ecology, I, Responses to the Physical Environment*, Vol. 12A, edited by O. L. Lange, P. S. Nobel, C. B. Osmond, and H. Ziegler, pp. 41-55, Springer-Verlag, New York, 1981.

McGill, W. B., H. W. Hunt, R. G. Woodmansee, and J. O. Reuss, A model of the dynamics of carbon and nitrogen in grassland soils, *Ecol. Bull.*, *33*, 49-116, 1981.

McGuire, A. D., J. M. Melillo, L. A. Joyce, D. W. Kicklighter, A. L. Grace, B. Moore III, and C. J. Vörösmarty, Interactions between carbon and nitrogen dynamics in estimating net primary production for potential vegetation in North America, *Global Biogeochem. Cycles*, *6*(2), 101-124, 1992.

Melillo, J. M., McGuire, A. D., D. W. Kicklighter, B. Moore III, C. J. Vörösmarty, and A. L. Schloss, Global climate change and terrestrial net primary production, *Nature*, *363*, 234-240, 1993.

Mintz, Y. and Y. Serafini, Global fields of soil moisture and land surface evapotranspiration, *NASA Tech. Memo. 83907*, 178-180, 1981.

Monteith, J. L., Solar radiation and productivity in tropical ecosystems, *J. Appl. Ecol.*, *9*, 747-766, 1972.

Monteith, J.L., Climate and efficiency of crop production in Britain, *Philos. Trans. R. Soc. London*, Ser. B, *281*, 271-294, 1977.

Mooney, H. A., B. G. Drake, R. J. Luxmoore, W. C. Oechel, and L. F. Pitelka, Predicting ecosystem responses to elevated CO_2 concentrations, *Bioscience*, *41*, 96-104, 1991.

Nadelhoffer, K. J., and J. W. Raich, Fine root production estimates and below ground carbon allocation in forest ecosystems, *Ecology*, *73*, 1139-1147, 1992.

Papendick, R. I., and G. S. Campbell, Theory and measurement of water potential, in *Water Potential Relations in Soil Microbiology*, pp. 1-22, Soil Science Society of America, Madison, Wis., 1980.

Parton, W. J., D. S. Schimel, C. V. Cole, and D. S. Ojima, Analysis of factors controlling soil organic matter levels in Great Plains grasslands, *Soil Sci. Soc. Am. J.*, *51*(5), 1173-1179, 1987.

Parton, W.J., A. R. Mosier, and D. S. Schimel, Dynamics of C, N, P, and S in grassland soils: A model, *Biogeochemistry*, *5*, 109-131, 1988.

Parton, W. J., C. V. Cole, J. W. B. Stewart, D. S. Ojima, and D. S. Schimel, Simulating regional

patterns of soil C, N, and P dynamics in the U.S. central grasslands region, in *Ecology of Arable Land*, edited by M. Clarholm and L. Bergstrom, pp. 99-108, Kluwer Academic, Higham, Mass., 1989a.

Parton, W. J., R. L. Sanford, P. A. Sanchez, and J. W. B. Stewart, Modeling soil organic matter dynamics in tropical soils, in *Dynamics of Soil Organic Matter in Tropical Ecosystems*, edited by D. C. Coleman et al., pp. 153-171, University of Hawaii Press, Honolulu, 1989b.

Parton, W. J., B. McKeown, V. Kirchner, and D. Ojima, *CENTURY Users Manual*, Natural Resource Ecology Laboratory, Colorado State University, Fort Collins, 1992.

Parton, W.J., D.S. Schimel, D. S. Ojima, and C. V. Cole, A general model for soil organic matter dynamics: Sensitivity to litter chemistry, texture and management, *Soil Sci. Soc. Am. J.*, in press, 1993.

Pastor, J., and W. M. Post, Calculating Thornthwaite's and Mather's actual evapotranspiration using an approximating function, *Can. J. For. Res., 14*, 466-467, 1984.

Pierce, L. T., Estimating seasonal and short-term fluctuations in evapotranspiration from meadow crops, *Bull. Am. Meteorol. Soc., 39*, 73-78, 1958.

Post, W. M., J. Pastor, P. J. Zinke, and A. G. Stangenberger, Global patterns of soil nitrogen storage, *Nature, 317*, 613-616, 1985.

Raich, J. W., E. B. Rastetter, J. M. Melillo, D. W. Kicklighter, P. A. Steudler, B. J. Peterson, A. L. Grace, B. Moore III, and C. J. Vörösmarty, Potential net primary production in South America: Application of a global model, *Ecol. Appl., 1*(4), 399-429, 1991.

Raich, J. W., and W. H. Schlesinger, The global carbon dioxide flux in soil respiration and its relationship to vegetation and climate, *Tellus*, Ser. B, *44*, 81-99, 1992.

Rastetter, E. B., M. G. Ryan, G. R. Shaver, J. M. Melillo, K. J. Nadelhoffer, J. E. Hobbie, and J. D. Aber, A general biogeochemical model describing the responses of the C and N cycles in terrestrial ecosystems to changes in CO_2, climate and N deposition, *Tree Physiol., 9*, 101-126, 1991.

Richter, D. D. and L. I. Babbar, Soil diversity in the tropics, *Adv. Ecol. Res., 21*, 315-389, 1992.

Rodin, L. E., and N. I. Bazilevich, *Production and Mineral Cycling in Terrestrial Vegetation*, Oliver and Boyd, Edinburgh, 1967.

Running, S. W., and J. C. Coughlan, A general model of forest ecosystem processes for regional applications, I, Hydrologic balance, canopy gas exchange and primary production processes, *Ecol. Modell., 42*, 125-154, 1988.

Russell, G. P. G. Jarvis, and J. L. Monteith, Absorption of radiation by canopies and stand

growth, in *Plant Canopies: Their Growth, Form and Function*, edited by G. P. Russell et al., pp. 21-39, Cambridge University Press, New York, 1989.

Ryan, M. G., Effects of climate change on plant respiration, *Ecol. Appl., 1*, 157-167, 1991.

Sala, O. E., W. K. Lauenroth, and I. C. Burke, Carbon budgets of temperate grasslands and the effects of global change, in *Global Change: Effects on Coniferous Forests and Grasslands*, edited by J. M. Melillo and A. Breymeyer, John Wiley, New York, in press, 1993.

Sanchez, P. A., M. P. Gichuru, and L. B. Katz, Organic matter in major soils of the tropical and temperate regions, *Trans. Int. Congr. Soil Sci., 12th, 1*, 99-114, 1982.

Saxton, K. E., W. J. Rawls, J. S. Romberger, and R. I. Papendick, Estimating generalized soil-water characteristics from texture, *Soil Sci. Soc. Am. J., 50*, 1031-1036, 1986.

Schlesinger, W. H., Carbon balance in terrestrial detritus, *Ann. Rev. Ecol. Syst., 8*, 51-81, 1977.

Schlesinger, W. H., *Biogeochemistry: An Analysis of Global Change*, pp. 443, Academic, San Diego, Calif, 1991.

Schowalter, T. D., Heterogeneity of decomposition and nutrient dynamics of oak (*Quercus*) logs during the first 2 years of decomposition, *Can. J. For. Res., 22*, 161-166, 1992.

Schulze, E. D., and F. S. Chapin III, Plant specialization to environments of different resource quality, in *Potentials and Limitations in Ecosystem Analysis*, edited E. D. Schulze and H. Zwolfer, pp. 120-148, Springer-Verlag, New York, 1987.

Sellers, P. J., Canopy reflectance, photosynthesis and transpiration, *Int. J. Remote Sens., 6*, 1335-1372, 1985.

Sellers, P. J., Canopy reflectance, photosynthesis and transpiration, II. The role of biophysics in the linearity of their interdependence. *Remote Sens. Environ., 21*, 143-183, 1987.

Sellers, P. J., J. A. Berry, G. J. Collatz, C. B. Field, and F. G. Hall, Canopy reflectance, photosynthesis and transpiration, III, A reanalysis using improved leaf models and a new canopy integration scheme, *Remote Sens. Environ., 42*, 187-216, 1992.

Sellers, P. J., S. O. Los, C. J. Tucker, C. O. Justice, D. A. Dazlich, G. J. Collatz, and D. A. Randall, A revised land surface parameterization (SIB-2) for atmospheric general circulation models. Part 2, The generation of global fields of terrestrial biophysical parameters from satellite data, *J. Clim.*, in press, 1993.

Sims, P. L., and R. T. Coupland, *Producers in Grassland Ecosystems of the World*, edited by R. T. Coupland, pp 49-72, Cambridge University Press, New York, 1979.

Sorenson, L. H., Carbon-nitrogen relationships

during humification of cellulose in soils containing different amounts of clay, *Soil Biol. Biochem., 13*, 313-321, 1981.

Squire, G. R., B. Marshall, and C. K. Ong, Development and growth of pearl millet (*Pennisetum typhoides* S. and H.) in response to water supply and demand, *Exp. Agric.*, 22, 289-300, 1986.

Stohlgren, T. J., Litter dynamics in two Sierran mixed conifer forests, I, Litterfall and decompostion rates, *Can. J. For. Res.*, *18*, 1127-1135, 1988.

Stott, D. E., L. F. Elliott, R. I. Papendick, and G. D. Campbell, Low temperature or low water potential effects on the microbial decomposition of wheat straw, *Soil Biol. Biochem., 18*(6), 577-582, 1983.

Taylor, B. R., and H. G. Jones, Litter decomposition under snow cover in a balsam fir forest, *Can. J. Bot., 68*, 122-120, 1990.

Thornthwaite, C. W., An approach toward rational classification of climate, *Geogr. Rev., 38*, 55-94, 1948.

Thornthwaite, C. W., and J. R. Mather, Instructions and tables for computing potential evapotranspiration and water balance, *Publ. Climatol., 10*, 185-311, 1957.

Tisdale, J. M., and J. M. Oades, Organic matter and water stable aggregates in soil, *J. Soil Sci., 33*, 141-163, 1982.

Titlyanova, A. A., and N. I. Bazilevich, Ecosystem synthesis of meadows: Nutrient cycling, in *Grassland Ecosystems of the World: Analysis of Grasslands and their Uses*. IBP 18, edited by R. T. Coupland, pp. 165-170, Cambridge University Press, New York, 1979.

Townsend, A. R., P. M. Vitousek, and E. A. Holland, Tropical soils dominate the short-term carbon cycle feedbacks to atmospheric carbon dioxide, *Clim. Change*, 22, 293-303, 1992.

Tucker, C. J., I. Y. Fung, C. D. Keeling, and R. H. Gammon, Relationship between atmospheric CO_2 variations and a satellite-derived vegetation index, *Nature*, *319*, 195-199, 1986.

Van Veen, J. A., J. N. Ladd, and M. J. Frissel, Modelling C and N turnover through the microbial biomass in soil, *Plant Soil, 76*, 257-274, 1984.

Vörösmarty, C. J., B. Moore III, A. L. Grace, M. P. Gildea, J. M. Melillo, B. J. Peterson, E. B. Rastetter, and P. A. Steudler, Continental scale models of water balance and fluvial transport: An application to South America, *Global Biogeochem. Cycles. 3*(3), 241-265, 1989.

Wofsy, S. C., M. L. Goulden, J. W. Munger, S.-M. Fan, P. S. Bakwin, B. C. Daube, S. L. Bassow, and F. A. Bazzaz, Net Exchange of CO_2 in a mid-latitude forest, *Science, 260*, 1314-1317, 1993.

Zahner, R., Refinement in empirical functions for realistic soil-moisture regimes under forest cover, in *Forest Hydrology*, edited by W. E. Sopper and H. W. Lull, pp. 261-274, Pergamon Press, New York, 1967.

Zobler, L. A., world soil file for global climate modeling, *NASA Tech. Memo., 87802*, 32 pp., 1986.

C. B. Field and J. T. Randerson, Carnegie Institution of Washington, Department of Plant Biology, 290 Panama Street, Stanford, CA 94305.

S. A. Klooster and C. S. Potter, Johnson Controls, NASA Ames Research Center, Mail Stop 239-20, Moffett Field, CA 94035.

P. A. Matson, NASA Ames Research Center, Mail Stop 239-20, Moffett Field, CA 94035.

H. A. Mooney and P. M. Vitousek, Department of Biological Sciences, Stanford University, Stanford, CA 94305.